Sustainable Food Technology

ROYAL SOCIETY OF CHEMISTRY

REVIEW

View Article Online
View Journal | View Issue

Cite this: *Sustainable Food Technol.*, 2025, **3**, 1681

Electronic tongue: active channels, molecular sieves, receptors and arrays

Hyuk Jin Kim, †[a] Jun Uh Hyun †[a] and Ho Won Jang *[ab]

Electronic tongues (E-tongues) have emerged as innovative sensing platforms that mimic the human gustatory system, enabling the precise analysis of complex chemical mixtures. Recent advances in E-tongue technologies have been driven by developments in four fundamental components: active channels, molecular sieves, receptors and arrays. These advancements contribute to enhanced sensitivity, selectivity and functionality in taste sensing systems. The atomic-scale thickness and high surface-area-to-volume ratios of two-dimensional (2D) materials, including graphene, MXenes and transition metal dichalcogenides, make them effective active channels that significantly improve sensitivity and selectivity. Analytes can be precisely separated and filtered from complex solutions using molecular sieves such as metal–organic frameworks, covalent organic frameworks and polymer membranes. Engineered receptors, which can be synthetic macrocyclic compounds or biological types such as enzymes and aptamers, enable targeted interactions with specific taste molecules. For real-time monitoring, sophisticated sensor arrays, including ion-sensitive field-effect transistors and triboelectric sensor arrays, convert chemical interactions into measurable electrical signals. By combining these advanced components, E-tongue systems can achieve unprecedented accuracy and reliability in a variety of applications, from environmental monitoring to biomedical diagnostics and food quality evaluation.

Received 26th May 2025
Accepted 31st July 2025

DOI: 10.1039/d5fb00237k

rsc.li/susfoodtech

Sustainability spotlight

With the growing demand for accurate and precise taste detection in food quality control, environmental surveillance and personalized healthcare, efficient screening of chemically complex liquids has become a central analytical challenge. We overview the recent developments in active channel designs, molecular sieve interfaces, receptors and sensor arrays that may further advance with research on E-tongues. Beyond classical potentiometric sensors employing polymeric membranes and voltammetric sensors using metallic or modified carbon electrodes, this review emphasizes how the hybridization of these elements unlocks powerful synergistic effects, sharpening selectivity, amplifying sensitivity and streamlining on-chip practicality. These integrated architectures promise real-time, multiplexed taste analytics, expanding E-tongue utility from lab benches to process monitoring and even wearable health diagnostics.

[a]*Department of Materials Science and Engineering, Research Institute of Advanced Materials, Seoul National University, Seoul 08826, Republic of Korea. E-mail: hwjang@snu.ac.kr*

[b]*Advanced Institute of Convergence Technology, Seoul National University, Seoul 08826, Republic of Korea*

† These authors contributed equally to this work.

Hyuk Jin Kim

Hyuk Jin Kim is currently a PhD candidate under the supervision of Prof. Ho Won Jang in the Department of Materials Science and Engineering at Seoul National University (SNU). He received his BS degree in Materials Science and Engineering, Seoul National University, in 2022. His research focuses on chemoresistive liquid sensors based on 2D materials for electronic tongues.

Jun Uh Hyun

Jun Uh Hyun is currently a PhD candidate under the supervision of Prof. Ho Won Jang in the Department of Materials Science and Engineering at Seoul National University (SNU). He received his BS degree in Chemistry, University of Illinois Urbana-Champaign, in 2023. His research focuses on chemoresistive liquid sensors based on 2D materials for electronic tongues.

1. Introduction

Taste perception is a fundamental process that plays a crucial role in various fields, including food quality management, biomedical diagnostics and environmental monitoring. The human gustatory system, which relies on specialized receptors to detect and distinguish between different taste molecules, has inspired the development of E-tongues. These bioinspired devices aim to mimic human taste perception by integrating advanced materials and technologies to achieve the precise detection and analysis of complex chemical mixtures. However, despite being bioinspired, current E-tongue systems fall short of fully mimicking the complexity and adaptivity of human taste perception. Future improvements in biomimetic design, multimodal sensing, and AI integration are expected to narrow the gap between artificial and biological taste sensing, improving the relevance to real sensory responses.[1] The ability of E-tongues to deliver quantitative, objective and repetitive assessments of taste-related substances has attracted significant interest.[2] E-tongues are increasingly used in food technology, where they enable rapid, non-destructive detection and discrimination of key compounds such as sugars, amino acids, fatty acids, peptides and volatile oils in a wide range of food samples. Recent advances allow precise monitoring of sweetness in beverages, fermentation metabolites and freshness indicators in dairy or seafood products.[3–7] Fig. 1a illustrates the increasing number of publications on E-tongues, highlighting the expanding scholarly interest in this field, while Fig. 1b outlines key milestones in E-tongue technology. This concept began in the 1980s when the utilization of sensor arrays for liquid analysis was first proposed.[1] In the 1990s, the concept of taste sensors was introduced, which has since advanced into refined devices, enabling the global market commercialization of E-tongue systems by the early 2000s.[2] Since then, research in this area has been actively pursued. In the 2010s, efforts focused on hybrid E-tongue applications and the miniaturization of E-tongue systems, and more recently, portable E-tongues have accelerated research in the field.[8,9] The four essential elements of E-tongue systems, namely, active channels, molecular sieves, receptors and sensor arrays, are the subject of this investigation. The detection of taste molecules by 2D active channels relies on efficient charge transfer, a mechanism enhanced by the atomic-scale thickness of materials and high surface-area-to-volume ratio at the material–liquid interface. In addition, 2D materials have electrical characteristics that can be modified for certain sensing applications using techniques such as chemical functionalization and layer control.[10–12] These characteristics include semiconducting properties and adjustable bandgaps. Real-time monitoring of dynamic taste profiles and rapid signal processing are made possible by their high charge carrier mobility. Furthermore, the mechanical flexibility of 2D materials allows their easier incorporation into flexible or wearable E-tongue devices, providing new opportunities for *in situ* and non-invasive taste sensing applications.[15,16] In addition to performance advantages, the use of 2D material-based E-tongues may offer sustainability benefits. Miniaturized sensors can lower the power usage and facilitate early-stage spoilage detection, helping to reduce food waste across the supply chain. However, the environmental cost of synthesizing these nanomaterials must be considered when aiming for sustainable sensor solutions.[11,17]

Due to their high porosity and chemical stability, materials such as polymer membranes, metal–organic frameworks (MOFs) and covalent organic frameworks (COFs) are well-suited to function as molecular sieves. In particular, because of their adjustable pore sizes and functional groups that enable the selective adsorption of analytes, MOFs and COFs are very useful.[18–20] Alternatively, polymer membranes offer strong mechanical properties and integration across a range of sensor platforms. Molecular sieves increase the accuracy and reliability of E-tongue systems in identifying taste substances by specifically filtering out interfering compounds.[11,21]

Advances in receptor engineering have further enhanced the sensitivity and selectivity of E-tongue systems by incorporating nanomaterials or biomolecular recognition elements. These innovations enable precise detection of target substances even in complex mixtures with multiple interfering species. E-tongues also require receptors, which allow selective interaction with particular analytes. Receptors in E-tongue systems can be divided into three main types, chemical, synthetic and biological receptors.[10,22] These classifications are based on the biological recognition mechanisms found in the human tongue. High sensitivity is provided by biological receptors such as enzymes, aptamers and antibodies because of their intrinsic affinity for target molecules.[23,24] Through specific chemical interactions, synthetic receptors, such as macrocyclic compounds, are made to selectively capture ions or tiny molecules.[12,25,26] Functionalized materials or molecularly imprinted polymers (MIPs) with selective binding sites for particular analytes are frequently used in chemical receptors.[27,28] Each type of sensor array, from ion-sensitive field-effect transistors (ISFET) to triboelectric sensors, operates on a unique principle

Ho Won Jang

Ho Won Jang is Full Professor in the Department of Materials Science and Engineering at Seoul National University. He earned his PhD from the Department of Materials Science and Engineering at Pohang University of Science and Technology in 2004. He worked as Research Associate at the University of Wisconsin–Madison from 2006 to 2009. Before he joined Seoul National University in 2012, he worked in Korea Institute of Science and Technology as Senior Research Scientist. His research interests include the synthesis of oxides, 2D materials and halide perovskites, and their applications in chemical sensors, nanoelectronics, solar water splitting cells, plasmonics, metal–insulator transition and ferroelectricity.

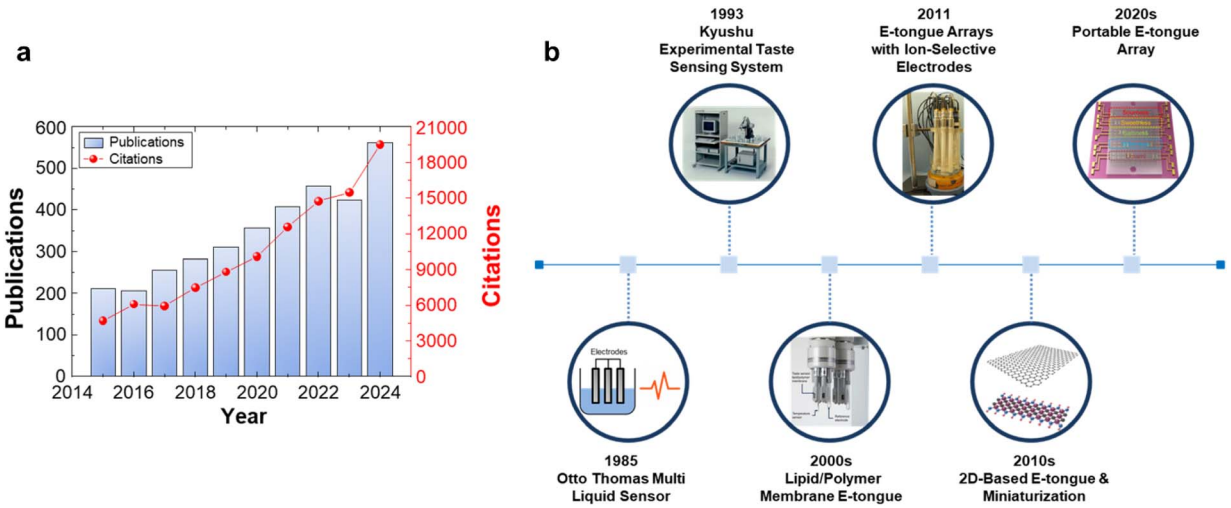

Fig. 1 (a) Annual number of publications related to E-tongues between 2015 and 2025 shows how this field has developed and attracted scholarly interest over time. The data was collected using the Web of Science: keywords (electronic tongue*) or (artificial taste*) were used. (b) Outline of important moments in E-tongue technology, from the 1985 release of the first liquid multi-sensor systems to the 2020s' portable E-tongue array. Significant developments are highlighted in the timeline, such as the invention of the experimental taste-sensing system in 1993, lipid/polymer membrane E-tongue in the 2000s and the 2D-based E-tongues & portable E-tongue array in the 2010s–2020s. Reproduced with permission from Intelligent Sensor Technology, ref. 13 and 14 Copyright 2011, MDPI.

to generate an electrical signal from analyte interactions. Analyte binding changes the surface potential, which ISFETs use to generate electrical signals with high sensitivity for measurement.[29,30] The detection of acidic or basic components in taste mixtures is most effectively achieved by pH sensor arrays, whereas triboelectric sensors use charge transfer mechanisms to identify physical interactions between analytes and sensor surfaces.[31,32] By combining these sensor arrays with advanced signal processing methods, E-tongues can handle complicated combinations with excellent accuracy and reliability. Furthermore, sensor array miniaturization enables portable, low-power E-tongue devices that reduce the dependence on bulky, energy-intensive lab equipment, enhancing sustainability in sensing technologies.[17,33] E-tongues have demonstrated exceptional performances in a variety of applications due to the combination of these four elements, *i.e.*, active channels based on 2D materials, molecular sieves for selective filtering, designed receptors for targeted detection and efficient sensor arrays. E-tongues are highly accurate in identifying chemicals or evaluating flavor profiles in food safety. For example, they are used to evaluate sweetness in beverages or detect spoilage markers in perishable foods. E-tongues provide a non-invasive platform for biomedical diagnostics, allowing the detection of biomarkers in physiological fluids such as urine and saliva. This capability is particularly valuable for monitoring diseases such as diabetes and kidney disorders through the detection of glucose and urea levels, respectively. Environmental monitoring also benefits from the ability of E-tongues to detect pollutants or hazardous chemicals in water sources with high sensitivity.[35,36]

However, despite these developments, there are still difficulties in maximizing the incorporation of these components into coherent systems that can function consistently in a variety of situations. For example, practical uses depend on the long-term stability of 2D materials in liquid settings. Research is also being done to increase the selectivity of molecular sieves, while preserving their high efficiency. To prevent deterioration over many use cycles, receptor design also has to find a balance between sensitivity and stability. The development of next-generation E-tongue technologies is being driven by recent developments in material design and system integration, which are highlighted in this analysis. Researchers are developing highly sensitive and selective taste sensors that can deal with important issues in contemporary science and technology by utilizing the distinctive characteristics of 2D materials in conjunction with advanced molecular sieves, engineered receptors and elaborate sensor arrays. These advancements have the potential to facilitate applications in environmental analysis, medical diagnostics, food safety and other fields.[1,10,35,37]

2. 2D materials for active channels

In E-tongue systems, 2D materials have emerged as exceptional candidates for the active channels. They are especially appropriate for liquid sensing applications because of their distinct structural and functional characteristics. Unlike conventional bulk materials, 2D materials offer an atomically thin structure that provides an extremely high surface-area-to-volume ratio.[10,13,16] At the material–liquid interface, this property is essential for enhancing molecular interactions and enabling effective charge transfer processes. The family of 2D materials, including graphene, TMDs and MXenes, offers a diverse range of electrical properties that can be modified to satisfy particular sensing requirements.[11,12,14] Since they are atomically thin, they are extremely sensitive to changes in the specific electrical environment, which makes them suitable for detecting even small amounts of taste components in solutions.[37,39]

Table 1 Comparative analysis of channel materials and detection methods for diverse target substances in E-tongue systems

Channel material	Target	Detection range	Measurement method	Response/recovery time	Reversibility (amperometric)	Sensitivity	Reference
Fluorinated graphene	Na^+	0.1 mM–1 M	Transfer curves, amperometric	~120 s, N/A	Irreversible	−55.4 mV dec^{-1}	34
Silicon nanowire	Na^+	0.1 mM–1 M	Transfer curves, amperometric	~90 s, N/A	Reversible	59.16 mV dec^{-1}	43
Au-coated silicon nanowire	Na^+	1 mM–1 M	Threshold voltage change by molarity	N/A, N/A	N/A	−44 mV dec^{-1}	44
Fluoro polysiloxane	Na^+	0.01 mM–1 M	Amperometric	50 s, N/A	Irreversible	57 mV dec^{-1}	45
Amorphous In–Ga–Zn–oxide	Na^+	1 mM–1 M	Amperometric	N/A, N/A	Reversible	60 mV dec^{-1}	46
Carbon black/silicone elastomer composite	Na^+	0.01 mM–1 M	Amperometric	~60 s, N/A	Reversible	56.1 mV dec^{-1}	47
Nafion/calix[4]arene/graphene	Na^+	100 nM–10 mM	Transfer curves, on-off available sensing curves	33 s, ~100 s	Reversible	5 mM: 690%	12
Graphene	pH	4–10 pH	Amperometric	5 s, 20 s	N/A	N/A	48
Graphene	pH	6–9 pH	Transfer curves, amperometric	N/A, N/A	Reversible	N/A	49
Graphene	pH	4.0–8.2 pH	Transfer curves, amperometric	~60 s, N/A	N/A	N/A	50
Epitaxial graphene	pH	2–12 pH	Transfer curves	N/A, N/A	N/A	98 mV pH^{-1}	51
Graphene mesh	pH	6.55–8.25 pH	Transfer curves	N/A, N/A	N/A	7 mV pH^{-1}	52
Graphene on HfO_2	pH	5.3–9.3 pH	Transfer curves, amperometric	~10 s, ~50 s	Reversible	58.2 mV pH^{-1}	53
Graphene	pH	4.3–8.4 pH	Transfer curves, amperometric	~50 s, ~100 s	Reversible	22 mV pH^{-1}	54
Au-decorated graphene	pH	5.55–8.05 pH	Transfer curves, on-off available sensing curves	~30 s, ~100 s	Reversible	115.2 mV pH^{-1}	10
ReS_2	pH	3.21–8.11 pH	Transfer curves, amperometric	N/A, N/A	Irreversible	54.8 mV pH^{-1}	55
Cu nanoparticle-modified graphene	Glucose	0.05–0.25 mM	Amperometric	~2 s, N/A	N/A	N/A	56
Graphene/AuNPs/chitosan nanocomposites	Glucose	2–10 mM	Cyclic voltammograms, amperometric	~10 s, N/A	N/A	6 mM: 3.2%	57
Pt NPs/graphene/chitosan nanocomposite film	Glucose	0.15–4.2 mM	Cyclic voltammograms, amperometric	~10 s, N/A	N/A	N/A	58
Graphene	Glucose	0.1–10 mM	Amperometric	~50 s, N/A	N/A	N/A	59
Au-Decorated graphene	Glucose	0.01–10 mM	Transfer curves, on–off available sensing curves	~50 s. ~125 s	Reversible	32 mV m M^{-1} 5 mM: 2750%	10
N-Doped graphene	Glucose	0.01–1.1 mM	Transfer curves, amperometric	N/A, N/A	Irreversible	N/A	60
Pt-GO	Glucose	2 μM–10.3 mM	Amperometric	N/A, N/A	Irreversible	0.64 μM mM^{-1} cm^{-2}	61 and 62
Mn_2O_3/Au	MSG	0–25%	SPR curve	~5 s, N/A	N/A	461.71 nm/%	63
MoS_2/Au	MSG	0.05 μM–200 mM	Electrochemical detection	~30 min, N/A	N/A	N/A	64

2.1. Why 2D materials?

2D materials have emerged as promising candidates as the active channels in E-tongue systems, offering distinct advantages over conventional bulk materials. The atomic-scale thickness of 2D materials provides an exceptionally high surface-area-to-volume ratio, maximizing the exposure of atoms to the surrounding environment. This property improves the interactions between the target analytes and the sensing material, which enhances the sensitivity for taste substances.[12,40] Many 2D materials have adjustable bandgaps and semiconducting behavior, among other controllable electrical characteristics. Their electrical characteristics can be optimized for particular taste sensing applications using methods such as chemical functionalization, strain engineering and controlling the number of layers. Rapid signal processing and fast reaction times are made possible by this tunability in conjunction with the high charge carrier mobilities observed in 2D materials. These characteristics are essential for the real-time monitoring of dynamic taste profiles under liquid conditions. Because many 2D materials are chemically stable in solution, they perform consistently in a variety of liquid conditions that can be observed in E-tongue applications.[2,11,41] Additionally, different chemical groups or biomolecules can easily be added to the surfaces of 2D materials, making it possible to create highly selective sensors for certain ions or taste molecules in complex mixtures. Another significant benefit of 2D materials is their mechanical flexibility, which allows them to be integrated into lightweight, wearable E-tongue devices. These features not only enhance the sensor performance but also contribute to sustainability by reducing the material usage and energy consumption during device fabrication. However, the scalable production and end-of-life disposal of advanced nanomaterials such as graphene, TMDs and MXenes remain important considerations for ensuring a net environmental benefit in E-tongue applications. As a result of their exceptional electrical conductivity and electron mobility, materials such as graphene and MoS_2 are expected to continue playing a pivotal role in the development of next-generation taste sensing platforms.[11,12] As research in this field progresses, 2D materials are expected to play an increasingly crucial role in the development of next-generation taste sensing technologies.[1,42]

2.2. 2D material-based taste sensors

The sensitivity, selectivity and practical utility of taste sensors have been greatly improved by the use of 2D materials. These materials, which include graphene, graphene oxide (GO), MoS_2, and MXenes, have special electrical and mechanical properties

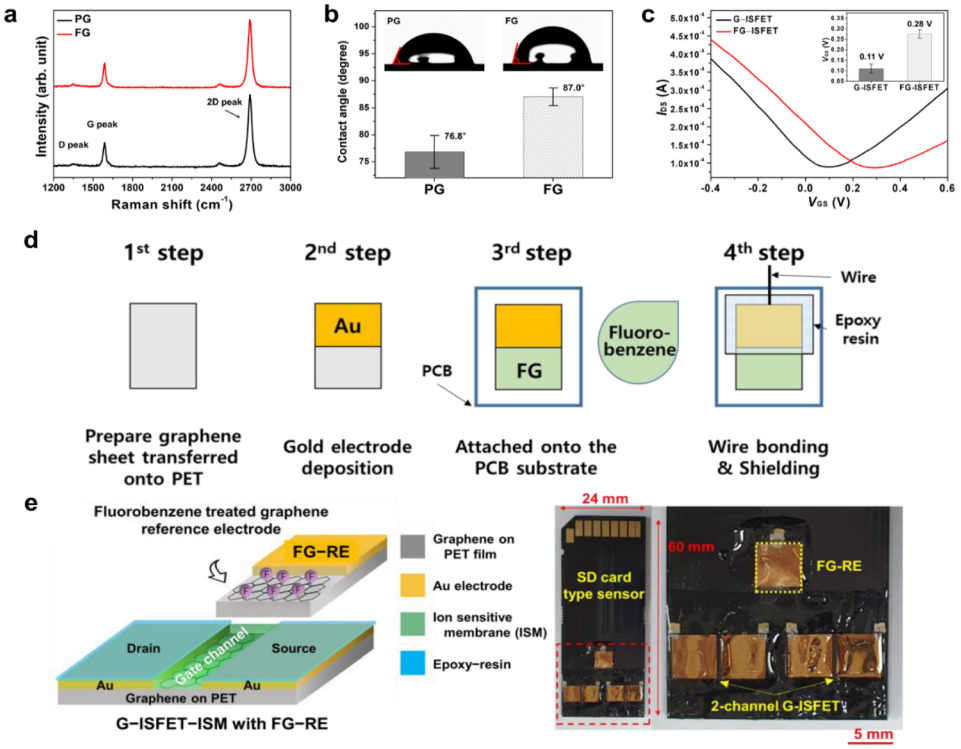

Fig. 2 Structural, surface and electrical characteristics of graphene before and after fluorobenzene treatment, along with the fabrication and integration of an FG-based sensing device. (a) Raman spectra of PG and FG, showing distinct G and 2D peaks for FG, indicating structural modifications induced by fluorobenzene treatment. (b) Water contact angle measurements reveal an increase in hydrophobicity after fluorobenzene treatment, with the contact angle increasing from 76.8° (PG) to 87.0° (FG). (c) Transfer characteristics (I_{DS}–V_{GS} curves) of the G-ISFET and FG-ISFET, highlighting the enhanced sensing performance of the FG-ISFET. (d) Fabrication steps of the FG-RE. (e) Schematic and photograph of the integrated sensing platform, showing the FG-RE and G-ISFET-ISM assembled on an SD card-type PCB. Reproduced with permission from ref. 34 Copyright 2021, MDPI.

that make them appropriate for enhancing the electrochemical performance in E-tongue systems (Table 1).[37,38,51]

Graphene has long been recognized for its exceptional electrical conductivity, mechanical flexibility and high surface area, making it a promising material for sensing applications. However, for sophisticated electrochemical sensing applications, pristine graphene (PG) frequently lacks the stability and selectivity needed. Fluorinated graphene (FG), which is produced through fluorobenzene treatment to overcome these constraints, introduces structural alterations and improves its characteristics for ion-sensing applications. The structural changes induced by fluorobenzene treatment are noticeable in the Raman spectra shown in Fig. 2a.[34,65] While the D, G and 2D peaks of FG are observed at similar positions to that of PG, the slight variations in their intensity ratios (I_D/I_G and I_G/I_{2D}) indicate minor modifications in the defect density and electronic structure. These changes suggest that fluorobenzene functionalization occurs through π–π interactions without interrupting the graphene lattice. Enhanced hydrophobicity is demonstrated through water contact angle measurements (Fig. 2b), where FG shows an increased contact angle of 87.0° compared to 76.8° for PG. This improved hydrophobicity contributes to greater stability in liquid environments, a critical factor for a reliable sensor performance.[49] FG-based ion-sensitive field-effect transistors (FG-ISFET) have a voltage offset of 0.28 V compared to 0.11 V for G-ISFET, according to their transfer characteristics (Fig. 2c).[66,67] This improvement is a result of the changed electrical characteristics of FG, which endow it with enhanced ion-sensing capabilities. Fig. 2d provides a step-by-step breakdown of the process for the fabrication of the FG reference electrodes (FG-RE), which includes graphene transfer onto polyethylene terephthalate (PET) substrates, gold electrode deposition, fluorobenzene treatment and epoxy resin encapsulation for durability. The integration of FG-RE and G-ISFET-ISM (ion-sensitive membrane) on an SD card-style printed circuit board (PCB) is finally shown in Fig. 2e.[30,68] With the use of ISFET technology and the increased sensitivity of FG, this platform functions as an effective ion-sensing device that can identify taste substances in complicated liquid environments.[34,69] These developments in fluorinated graphene technology will enable E-tongue systems to detect taste molecules with improved sensitivity, stability and reliability, enabling applications in biomedical diagnostics, environmental monitoring and food quality control.

GO and silver nanoparticles (AgNPs) have distinctive properties, which have been used to produce an AgNP/GO nanocomposite sensor, a highly efficient sodium ion (Na^+) detection device. The produced nanocomposite is drop-casted onto the working electrode (WE) of a screen-printed silver electrode (SPE), as shown in Fig. 3a, which depicts the manufacturing process.[38] A carbon counter electrode (CE) and an Ag/AgCl reference electrode (RE) are part of the SPE design, which ensures accurate electrochemical measurements. Its electrochemical performance is demonstrated through cyclic

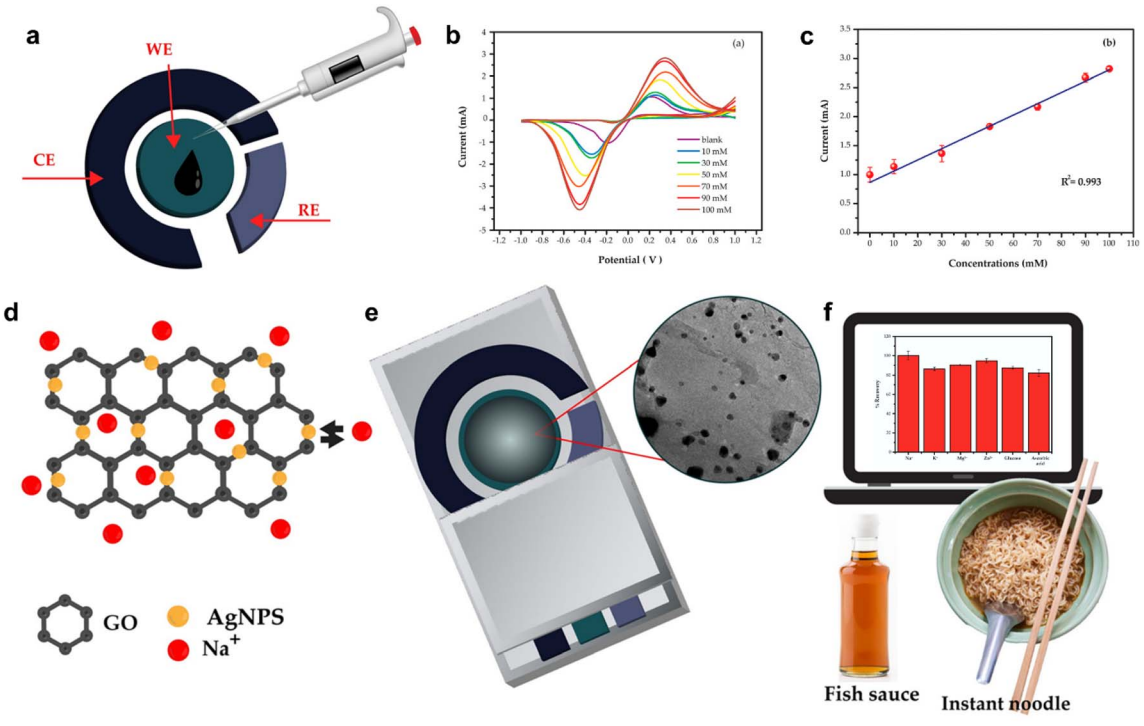

Fig. 3 Fabrication, characterization and performance of the AgNP/GO/SPE sensor for Na^+ detection. (a) Schematic representation of the fabrication process of the AgNP/GO/SPE sensor. (b) Cyclic voltammograms showing anodic peak currents for varying Na^+ concentrations. (c) Calibration curve demonstrating a linear relationship with an R^2 value of 0.993. (d) Schematic illustrating the preparation of the AgNP/GO nanocomposite. (e) Transmission electron microscopy (TEM) image of the synthesized AgNP/GO nanocomposite. (f) Selectivity test confirming Na^+ detection against potential interfering substances. Reproduced with permission from ref. 38 Copyright 2020, MDPI.

voltammetry curves in Fig. 3b, which show distinct anodic peak currents corresponding to varying Na^+ concentrations ranging from 10 mM to 100 mM. The calibration plot in Fig. 3c confirms a linear relationship between the current and Na^+ concentration, with an R^2 value of 0.993, indicating high sensitivity and reliability.[38,70] This linearity highlights the ability of this sensor to provide accurate quantification of Na^+ in complex solutions. Fig. 3d shows how GO and AgNPs interact molecularly, with GO behaving as the substrate for the deposition of AgNPs. AgNPs improve the catalytic characteristics, while the wide surface area of GO assists in ion adsorption, resulting in a hybrid nanomaterial with improved electrochemical properties for Na^+ detection. AgNPs are uniformly distributed on the GO surface, as seen in the TEM images in Fig. 3e. This further confirms the structural stability of the material and its role in improving the sensing performance. Fig. 3f illustrates the results of the chronoamperometric selectivity experiments that compare the response of the sensor to possible disturbing chemicals including glucose, K^+, Ca^{2+} and Mg^{2+} in a 50 mM Na^+ solution.[71] The high selectivity for Na^+ detection under appropriate measurement conditions is confirmed by the results, which show little interference from these compounds.[41] This novel sensor design provides an effective foundation for Na^+ detection by combining the catalytic efficiency of AgNPs with the large surface area and functional adaptability of GO.[38] Its potential as a crucial part of advanced E-tongue systems is demonstrated by its superior sensitivity, reliability and selectivity, which make it appropriate for practical applications such as environmental analysis and food quality monitoring.

MoS_2–PANI (polyaniline) composites have been developed as highly effective materials for pH sensing applications due to their unique structural and electrochemical properties. Using field emission scanning electron microscopy (FESEM), the shape of exfoliated MoS_2 nanosheets is shown in Fig. 4a. This layered structure is appropriate for the generation of composites.[40] Low-magnification TEM images (Fig. 4b) verify that PANI layers were successfully integrated onto MoS_2 nanosheets, while high-magnification TEM images (Fig. 4c) demonstrate that PANI is uniformly distributed on the nanosheet surfaces, improving the electrochemical activity of the composite.[34] Bulk

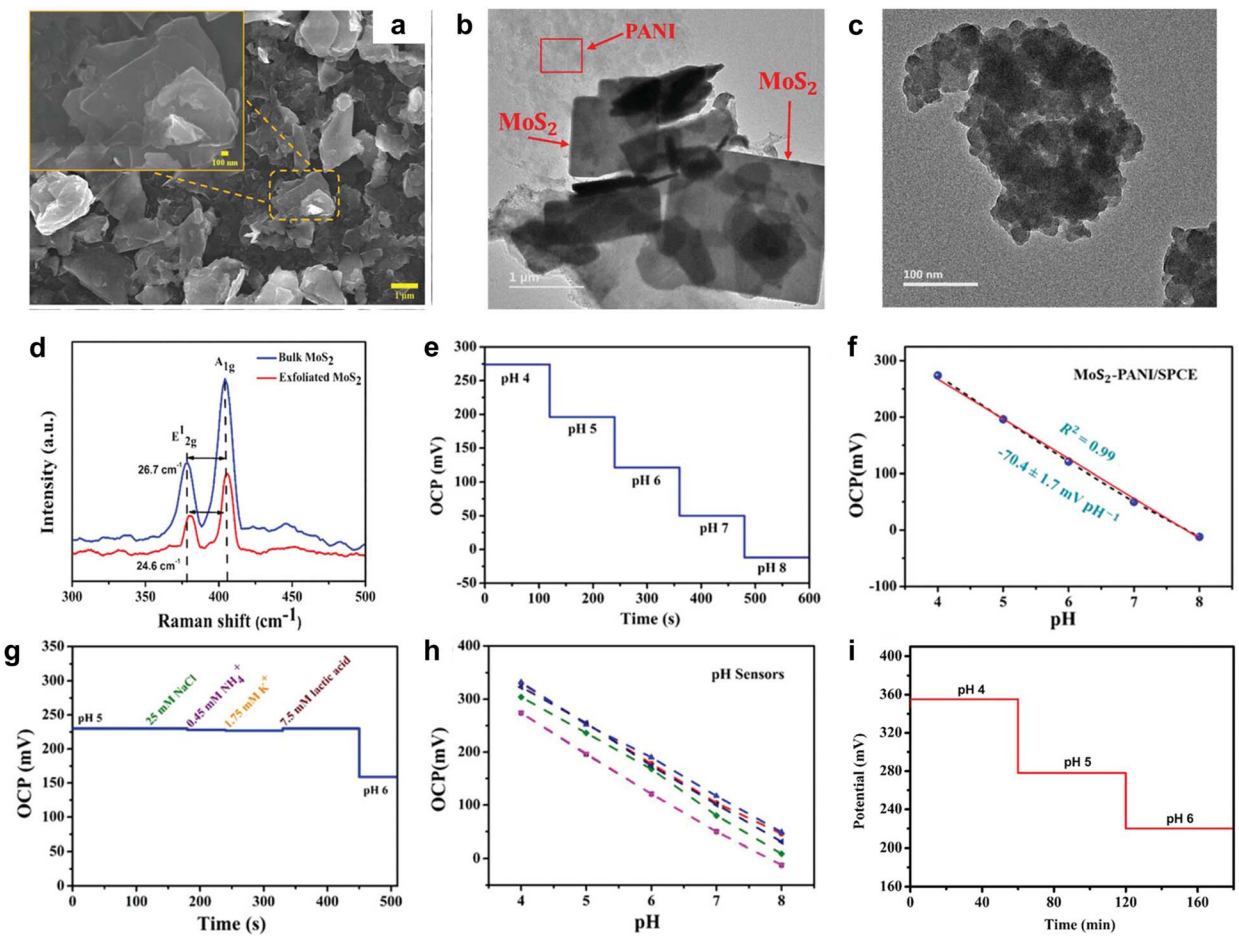

Fig. 4 Characterization and performance evaluation of the MoS_2–PANI/SPCE pH sensor. (a) FESEM image showing the morphology of exfoliated MoS_2 nanosheets. (b) and (c) TEM images illustrating the integration of PANI on MoS_2 nanosheets, with its uniform distribution enhancing the electrochemical properties. (d) Raman spectra indicating structural differences between exfoliated and bulk MoS_2. (e) and (f) OCP measurements demonstrating pH detection with a linear response ($R^2 = 0.99$). (g) Selectivity test reveals that competing ions such lactic acid, Na^+, NH_4^+ and K^+ have a negligible impact. (h) Reliability test that verifies that OCP-pH readings from various sensors are consistent. (i) Stability test confirming consistent performance throughout long pH detection times. Reproduced with permission from ref. 40 Copyright 2023, Wiley-VCH.

and exfoliated MoS_2 can be distinguished using Raman spectra (Fig. 4d), which show structural variations such as peak shifts in the A_{1g} and E_{2g} modes. These changes suggest that exfoliated MoS_2 has less interlayer coupling, which enhances its sensitivity in sensing applications. Measurements of open-circuit potential (OCP) (Fig. 4e) indicate that the sensor can identify pH variations in buffer solutions with a pH in the range of 4 to 8.[72,73] High stability and repeatability under a range of circumstances are demonstrated by the gradual changes in OCP. The high accuracy of the sensor is validated by the calibration plot (Fig. 4f), which shows a linear relationship between OCP and pH with a good correlation coefficient ($R^2 = 0.99$). In the presence of possible interfering chemicals including lactic acid, Na^+, NH^{4+} and K^+, selectivity tests (Fig. 4g) were carried out. The high selectivity of the sensor for H^+ ions is demonstrated by the negligible impact of these substances on OCP. Their stability for real-world applications is confirmed by reliability tests (Fig. 4h), which display consistent OCP-pH responses across various sensors.[73] All these results demonstrate that MoS_2–PANI/SPCE sensors effectively detect pH changes with excellent sensitivity, selectivity and stability.[40,74] The layered structure of MoS_2 and the electrochemical activity of PANI combine to make this composite a potential option for complex E-tongue systems used in environmental investigations, biomedical diagnostics and the monitoring of food quality.

3. Molecular sieves

Molecular sieves are structured materials with uniformly sized pores that separate substances based on shape or dimensions. Their origins can be traced to naturally occurring minerals, such as zeolites, which have a high internal surface area and a crystalline framework with consistent pore diameters. These features allow molecular sieves to selectively permit or exclude both molecules and ions. Considering the aforementioned ability, employment of molecular sieves may notably enhance the overall performance of E-tongue systems, which includes improvement in both selectivity and sensitivity, allowing them to remain as strong candidates as taste-sensing materials.

3.1. Role of molecular sieves

The sieving mechanism relies on a balance between steric hindrance and electrostatic interactions. When ion-containing fluids come into contact with a sieving layer, the ions smaller than or suitably shaped to match the pore openings can migrate through it, whereas larger ions are excluded.[75] Additionally, the presence of charged or functional groups on the pore walls can promote electrostatic interactions, further discriminating among ions of similar size but differing valence states or polarities.[76] As a result, E-tongues are able to measure even subtle changes in ionic concentrations, translating these differences into more reliable output signals. This precise molecular sieving is especially important when the detection of small ions or molecules, including protons or alkali metals, is necessary. In many E-tongue configurations, responding to variations in pH or sodium concentration is the key to characterizing sourness and saltiness. By incorporating molecular sieves, the device can selectively facilitate or hamper the flow of particular ions to the transducing elements of the sensor. This consistent, reproducible control over ion permeability enhances the overall signal-to-noise ratio (SNR) and minimizes cross-interference among different taste components. Additionally, molecular sieves improve the operational stability of the sensor array. By blocking large or unwanted molecular species, molecular sieves minimize the deposition of interfering compounds on the electrode surfaces. This feature can allow E-tongues to be employed for the long-term measurement of complex real-world samples. The design and fabrication of molecular sieves for E-tongue applications often integrate tunable membranes or frameworks, whereby pore size and surface functionalities can be adapted to match target ion dimensions and charge properties. Whether used in the form of MOFs, COFs or polymer membranes, molecular sieves elevate the sensitivity and selectivity of E-tongues. As a result, molecular sieves allow enhanced taste profiling, strengthening the overall role of E-tongues in various applications including food quality control, environmental monitoring and biomedical diagnostics.

3.2. MOFs, COFs and polymer membranes for molecular sieves

Molecular sieves have become increasingly prominent in the development of E-tongues. Traditional E-tongues rely on arrays of partially selective sensors to discriminate among complex taste modalities including sweet, bitter, sour, salty and umami. However, to improve the selectivity and sensitivity, researchers have investigated materials that combine well-defined porosity, chemical tunability and mechanical robustness. By leveraging these properties, MOFs, COFs and polymer membranes can better address the challenges associated with taste detection. Among the molecular sieves, MOFs stand out for their highly tunable architectures.[20] They typically feature inorganic metal nodes connected by organic ligands, forming robust crystalline networks, providing multiple advantages. Since these frameworks boast large internal surface areas and adjustable pore dimensions, the size-selective adsorption of diverse taste compounds can be achieved. Furthermore, their organic linkers can be functionalized to introduce specific recognition sites or to enhance their compatibility with biological or synthetic receptors. These features enable MOFs to act as highly sensitive sorbents in E-tongue applications, facilitating the accurate analysis of complex mixtures and improving the overall performance of E-tongue.

One example was reported by T. Lee *et al.*, where a photoluminescent MOF including $[In(OH)(bdc)]_n$ (bdc = 1,4-benzenedicarboxylate) and the Tb-based MOF-76 were used to differentiate the five basic tastants (sucrose, caffeine, citric acid, sodium chloride (NaCl) and monosodium glutamate (MSG)) in aqueous solutions.[76] Poly(acrylic acid) (PAA) was introduced on the surface of $[In(OH)(bdc)]_n$ to mimic taste receptor cells, and exposing the material to 10^{-2} M solution of each tastant led to protonation or deprotonation and ion-binding events that

altered its photoluminescence (PL). As a result, clear emission shifts were observed at 344 nm, 436 nm, 347 nm, 394 nm, and 335 nm for sucrose, caffeine, citric acid, NaCl and MSG, respectively. Meanwhile, the Tb-based MOF-76 harnessed the $5D_4 \rightarrow {}^7F_j$ transitions of terbium, producing a log-linear correlation in PL intensity reflecting the Weber–Fechner law. Then, a three-dimensional principal component analysis (3D-PCA) was conducted for taste discrimination, and clear grouping of each taste into distinct clusters was observed from the result.[75] Separately, X. Zhang *et al.* demonstrated a yolk–albumen–shell structure of mixed Ni–Co oxide with an ultrathin carbon shell for nonenzymatic glucose sensing.[77] For the synthesis of the material, a bimetallic Co–Ni MOF was initially synthesized, and then pyrolysis was conducted to obtain Ni–Co–O nanoparticles uniformly coated with a carbon shell with a thickness of about 2 nm. Notably, the final electrode showed high activity for glucose detection. The system exhibited a sensitivity of 1964 μA cm^{-2} mM^{-1} and a detection limit of 0.75 μM. In addition, its linear range extended from 5 μM to 1000 μM, and measurements were stable over repeated tests. This performance is partly attributed to the synergistic effect of Ni and Co oxide nanoparticles, as well as the increased surface area from the ultrathin carbon layer. The success of this Ni–Co oxide carbon composite highlights that bimetallic MOFs can provide a route for the rational design of porous nanocomposites for E-tongues.

Wang *et al.* introduced an $Ni_3(HITP)_2$-based field-effect transistor (FET) device for the selective detection of gluconic acid.[20] Fig. 5a and b show a schematic illustration of the Ni-MOF-FET with various gluconic acid concentrations. Their strategy involved the *in situ* growth of $Ni_3(HITP)_2$ membranes on a patterned Si/SiO_2 wafer bearing Au electrodes, carried out by suspending the substrate in a 65 °C reaction solution for up to 60 min. The prepared Ni-MOF was characterized by SEM, TEM, and HRTEM, as shown in Fig. 5c–f. The resulting thin film was both dense and porous, with a tunable thickness from about 190 nm to over 500 nm by adjusting the reaction time. Under ambient conditions, the Ni-MOF-FET exhibited a hole mobility up to 45.4 cm^2 V^{-1} s^{-1}, an on/off ratio of 2.29 × 10^3 and stable liquid-gated operation in phosphate-buffered saline with pH of 7.4. As shown in Fig. 5i and j, they monitored gluconic acid concentrations from 10^{-6} g mL^{-1} to 10^{-3} g mL^{-1} *via* source-drain current changes, where larger analyte concentrations suppressed channel conduction due to positive-charge adsorption on the $Ni_3(HITP)_2$ channel, effectively reducing hole accumulation. Thus, the high surface area and ordered porosity of $Ni_3(HITP)_2$ facilitated analyte binding and maintained a good FET performance. This highlights the advantage of combining the inherent porosity of MOFs with transistor readouts for enhanced selectivity and sensitivity of E-tongues.

Considering its usage in wide array of fields including biomedicine, chemical industries, cosmetics, fossil fuel and the food industry, ethanol sensing in a solution may also broaden the applications of E-tongues.[78] Therefore, ethanol sensors have been researched to fulfill the requirements of diverse fields. Lu *et al.* constructed a highly sensitive ethanol sensor by integrating a no-core fiber (NCF) with MOF nanofilms.[79] Specifically, they employed ZIF-8 films grown *in situ* on the surface of two NCF segments spliced to a single-mode fiber (SMF), forming an NSN architecture. In this design, multimode interference (MMI)

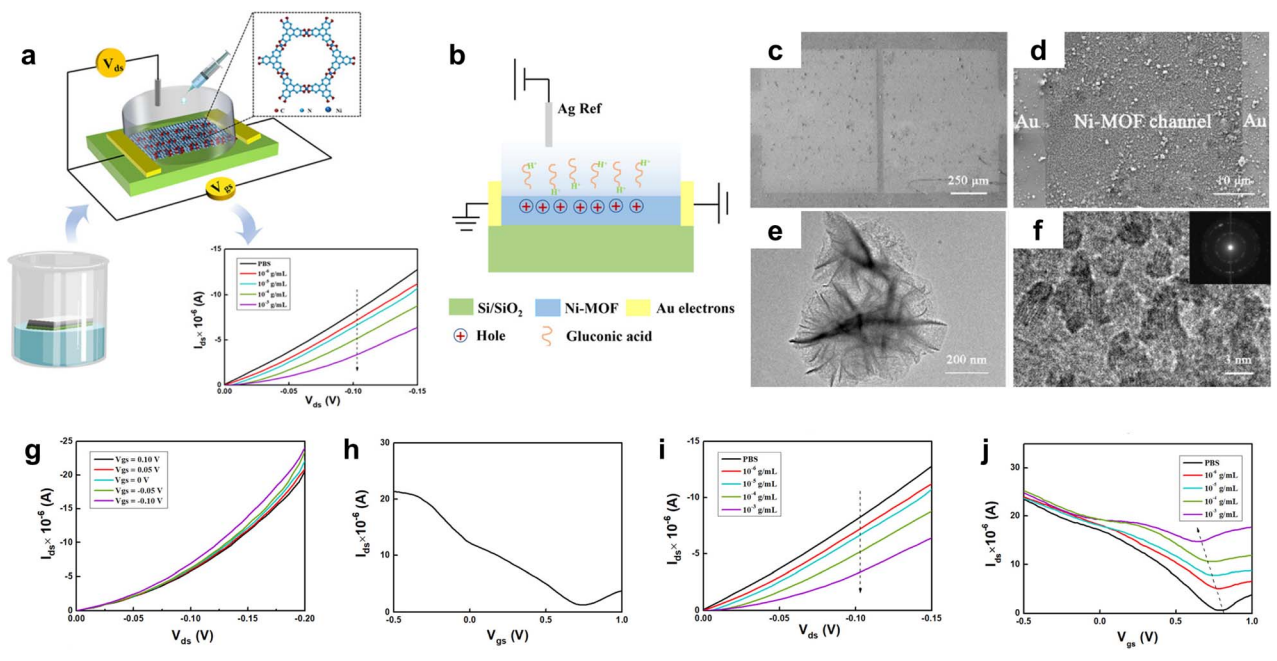

Fig. 5 Schematic of the overall working principles of the Ni-MOF-FET (a) as a liquid-gated FET and (b) detecting gluconic acid under a negative gate voltage. SEM images of (c) Ni-MOF-FET and (d) morphology of Ni-MOF reacting in channel. (e) TEM and (f) HRTEM images of the Ni-MOF, inset: selected area diffraction pattern. (g) I_{ds}–V_{ds} plots and (h) I_{ds}–V_{gs} plots (V_{ds} = −0.1 V) of the Ni-MOF-FET under PBS solution. (i) I_{ds}–V_{ds} plots (V_{ds} = −0.05 V) and (j) I_{ds}–V_{gs} plots (V_{ds} = −0.1 V) of the Ni-MOF-FET exposed to gluconic acid from 10^{-6} to 10^{-3} g mL^{-1}. Reproduced with permission from ref. 20 Copyright 2019, the American Chemical Society.

within the NCF was exploited to magnify the minute refractive index shifts caused by ethanol molecules adsorbed in the pores of ZIF-8. This system exhibited a sensitivity of 1.522 $nm\%^{-1}$ for ethanol concentrations up to 95% in water and maintained a limit of detection around 0.90%. By rinsing in deionized water, the device recovered its baseline, showing good reversibility after multiple tests. Additionally, the robust, uniform ZIF-8 coating enabled the straightforward fabrication of an optical sensor with high response to analytes. This approach demonstrates how the well-defined pore structures of MOFs can selectively preconcentrate analytes in an optical waveguide setting, enabling the rapid detection of tastes with high reliability. The ongoing study of MOFs in taste sensing highlights the valuable role of molecular sieves in E-tongue technology. Their porosity, adjustable surface features and inherent luminescence make them promising materials for next-generation E-tongues.[79,80] Although previous studies have demonstrated the potential of MOFs in E-tongue technology, further research could bring substantial improvement in the current E-tongue systems, potentially enabling more precise evaluations in areas such as food quality control and pharmaceutical analysis.

In addition to the research described above, recent progress has further highlighted the adaptability of COFs in various E-tongue applications. Because COFs consist of purely organic building blocks assembled through robust covalent linkages, they often exhibit enhanced chemical stability and can be readily functionalized with receptor molecules. The precise arrangement of pores in COFs not only supports size-selective recognition, but also facilitates efficient analyte transport, enabling faster sensor response times. Moreover, their intrinsic tunability permits researchers to engineer COFs to target a variety of tastes. Consequently, COFs can effectively serve as molecular sieves in E-tongue devices, merging high selectivity, quick signal readout and remarkable mechanical and chemical

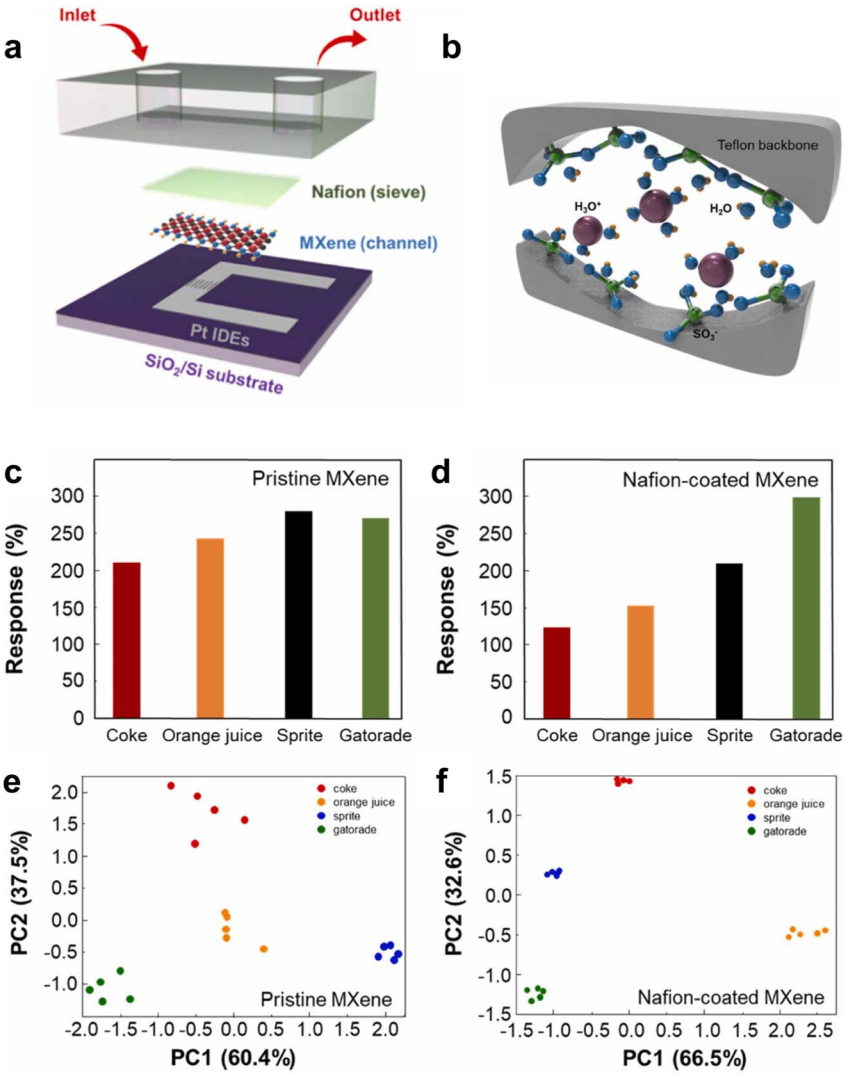

Fig. 6 (a) Schematic of the Nafion-coated MXene-based microfluidic channel-integrated pH sensor. (b) Ionic transfer mechanism of the Nafion sieve for selectively detecting H_3O^+. Response comparison of (c) the pristine MXene sensor, (d) Nafion-coated MXene sensor to four soft drinks (Coke, orange juice, Sprite and Gatorade). PCA plots of (e) pristine MXene sensor and (f) Nafion-coated MXene sensor for actual beverages. Reproduced with permission from ref. 11 Copyright 2024, Elsevier.

durability. Liang *et al.* reported the construction of Ni/NiO/carbon foam derived from a COF precursor by first coating a sacrificial silica template with a COF material, and then pyrolyzing the composite to form nitrogen-doped carbon foam embedded with Ni/NiO nanoparticles.[78,82] After etching the silica template, the resulting cellular carbon framework contained well-dispersed Ni/NiO particles, which acted as effective electrocatalysts with sieving ability for non-enzymatic glucose sensing. The sensor achieved a detection limit as low as 0.2 μM, a linear detection range from 0.6 mM to 8.6 mM and a sensitivity of 76.03 μA mM^{-1} cm^{-2} for glucose in alkaline solution. The hierarchical porosity and large surface area of the COF-derived foam led to enhanced electron transfer, reproducibility and operational stability, making it well-suited for practical applications.[82]

Yue *et al.* developed a colorimetric glucose sensor by covalently immobilizing glucose oxidase (GO_x) onto a carboxyl-functionalized COF.[83] In this system, the enzyme-coupled COF exhibited a linear response from 0.005 mM to 2 mM for glucose and displayed a limit of detection as low as 0.54 μM. This colorimetric method relies on the GO_x-mediated oxidation of glucose to generate hydrogen peroxide, which subsequently triggers a visible color change *via* a chromogenic substrate and horseradish peroxidase. Notably, the COF scaffold preserved over 85% of the original activity of the enzyme, even after 100 days of storage, showed improved temperature and pH resilience and enabled straightforward reuse. This robust design allowed the accurate quantification of glucose concentrations in complex samples such as body fluids and commercially available beverages, demonstrating the feasibility of enzyme-COF hybrids in practical applications, such as solution-phase diagnostic applications. While MOFs and COFs provide size-selective interactions and chemical stability for E-tongues, polymer-based membranes give an extra layer of molecular control and mechanical robustness. In particular, Nafion has become a widely used ion-conducting film. Its engineered structure allows small cations such as H^+ and Na^+ to move easily, while blocking larger or multicharged molecules. As a result, Nafion not only shields the underlying transducer from fouling or oxidative damage, but also enhances the selectivity and reproducibility in liquid-phase detection. MOFs and COFs, with their high porosity and tunable chemistry, allow highly selective detection with minimal reagent consumption, contributing to reduced chemical waste in analytical workflows. Nonetheless, the energy-intensive synthesis and potential challenges in recycling these frameworks highlight the need for lifecycle assessments in sustainable sensor design. When these membranes are integrated into E-tongues, the resulting systems quantify various tastants in real time across broad concentration ranges with enhanced overall performances.[80,81]

Kim and co-workers used a Nafion-coated Ti_3C_2 MXene film as the core sensing layer in a microfluidic device for real-time pH detection.[11] Fig. 6a shows a schematic image of the Nafion-coated MXene-based channel. Their approach combined an interdigitated electrode (IDE) with a Nafion coating on top of the MXene, followed by the integration of a PDMS microfluidic channel. As shown in Fig. 6b, because the Nafion membrane allows proton transport while rejecting larger species, the resulting sensor achieved a rapid response within a few seconds, along with excellent reversibility after multiple cycles of acid/base washing. The authors reported stable pH resolutions across a pH range of 5.5–8, with the minimal baseline drift attributed to robust ion-exchange capabilities of Nafion. Furthermore, the Nafion top layer was able to extend the sensor lifetime by preventing the oxidation of the MXene surface. This design achieved the necessary criteria for E-tongue applications by offering repeatable calibrations, a reproducible slope and negligible signal degradation over multiple days of testing. Ultimately, as shown in Fig. 6c–f, enhanced selectivity was observed from the Nafion-coated MXene sensor than the pristine MXene sensor upon the comparison of their response and principal component analysis (PCA) plots.[11]

In a subsequent report, Lee *et al.* proposed a dual-mode E-tongue where Nafion-coated graphene targeted pH sensing and Au-decorated graphene targeted glucose.[10] Nafion was spin-coated onto the graphene channel to form a film with a thickness of 280 nm, permitting small cations such as H^+ to pass, while blocking molecules such as ascorbic acid and uric acid. This allowed the sensor to exhibit a near-linear pH response from pH 5.5–8.1 with a slope of up to 1.05 $[pH]^{-1}$ and rapid response time of 13 s, which was nearly three-times faster than the average response time observed from the uncoated graphene. By contrast, the Au-decorated sensor excelled at glucose detection in the range of 0.01 mM to 10 mM, capitalizing on the catalytic electron transfer at the Au sites. Together, these findings support the notion that polymer membranes such as Nafion, combined with carefully chosen surface modifications, can yield robust multi-taste E-tongue arrays.

MOFs and COFs, with their high porosity and customizable chemistries, deliver high sensitivity and analyte-specific interactions, which are properties well-suited for detecting complex taste components in E-tongues. Alternatively, polymer membranes such as Nafion act as ion-selective barriers that further refine the selectivity, prevent sensor fouling and ensure stable baselines under repeated use. When these frameworks and/or membranes are integrated into E-tongues, the resulting systems quantify various tastants in real time across broad concentration ranges with enhanced overall performances. Therefore, considering their advantageous aspects, ongoing research on MOFs, COFs and polymer membranes as molecular sieves holds significant promise for the further advancement of E-tongue technology.

4. Receptors

Improving the sensitivity and selectivity of E-tongue devices requires careful consideration of receptor design and selection. Even in complicated mixtures with several interfering species, these receptors enable the precise detection of target substances such as ions, glucose and other biomolecules by promoting certain molecular interactions at the device surface. Thus, the reliability and efficiency of E-tongue systems in a variety of fields, such as pharmaceutical studies, environmental analysis, medical diagnosis and food quality

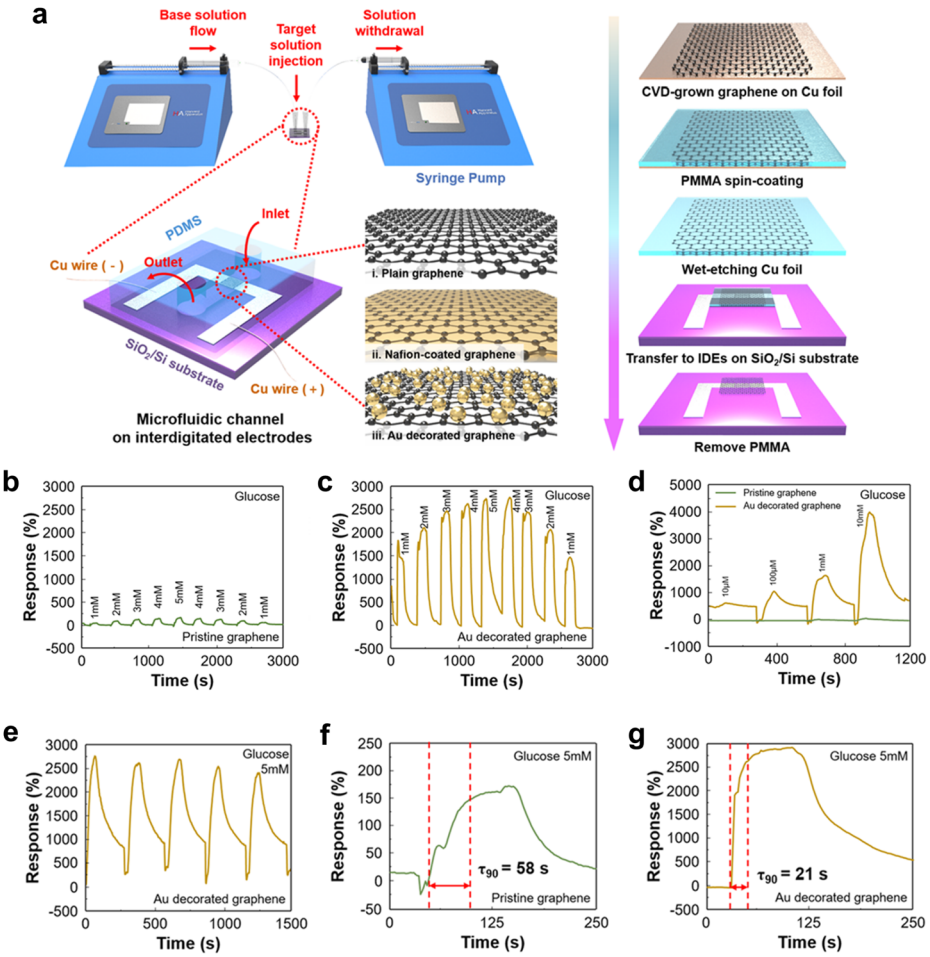

Fig. 7 Illustration and performance of an Au-decorated graphene microfluidic glucose detection device. (a) Design of the sensing device with IDEs and sensing materials on an SiO_2/Si substrate. Responses to glucose detection for pristine and Au-decorated graphene (b) and (c), demonstrating increased sensitivity with decorated Au nanoparticles. (d) Comparison of pristine and Au-decorated graphene detection limit tests. (e) High stability and reliability for glucose sensing are shown by repetitive response curves. Compared to pristine graphene, Au-decorated graphene displayed faster response kinetics (f) and (g). Reproduced with permission from ref. 10 Copyright 2021, Springer Nature.

monitoring, are greatly enhanced by receptor-based sensing systems.[12,25] Recent advances in receptor engineering have further expanded the capabilities of E-tongue systems by incorporating nanomaterials, biomolecular recognition elements and polymer-based selective coatings. These innovations have enabled the development of highly sensitive and selective sensors capable of real-time monitoring and precise measurements of target analytes under diverse conditions.

4.1. Role of receptors

In E-tongue systems, receptors are the main components of recognition, converting certain chemical interactions into measurable signals. They are specifically designed to improve the sensitivity and selectivity of devices that detect target substances such as Na^+ and glucose.[84] The fabrication and performance of a microfluidic glucose sensor using gold nanoparticles (AuNPs) as the receptor material are demonstrated in Fig. 7. The schematic in Fig. 7a shows the microfluidic channel integrated with IDEs on an SiO_2/Si substrate. The fabrication process involves transferring CVD graphene onto IDEs, followed by decoration with AuNPs. The glucose detection response using pristine graphene (Fig. 7b) shows limited sensitivity, whereas Au-decorated graphene (Fig. 7c) demonstrates significantly enhanced responses across varying glucose concentrations. The higher sensitivity of Au-decorated graphene over pristine graphene was confirmed by detection limit measurements (Fig. 7d). Furthermore, repeating response curves (Fig. 7e) demonstrate great stability and reliability for glucose sensing. Additionally, Au-decorated graphene exhibits faster response kinetics (Fig. 7f and g) in comparison to pure graphene.[10,56,58]

Fig. 8 focuses on Na^+ detection using Nafion/calix[4]arene/graphene sensors. The formation of an electric double layer (EDL) on the graphene surface is shown schematically in Fig. 8a. Counter ions (Cl^-) form a diffuse layer, while Na^+ ions are adsorbed into the Stern layer. Nafion selectively transports small cations, while calix[4]arene interacts specifically with Na^+ through oxygen atoms (Fig. 8b), enhancing the selectivity.[85,86] Long-term stability tests (Fig. 8c) demonstrate consistent

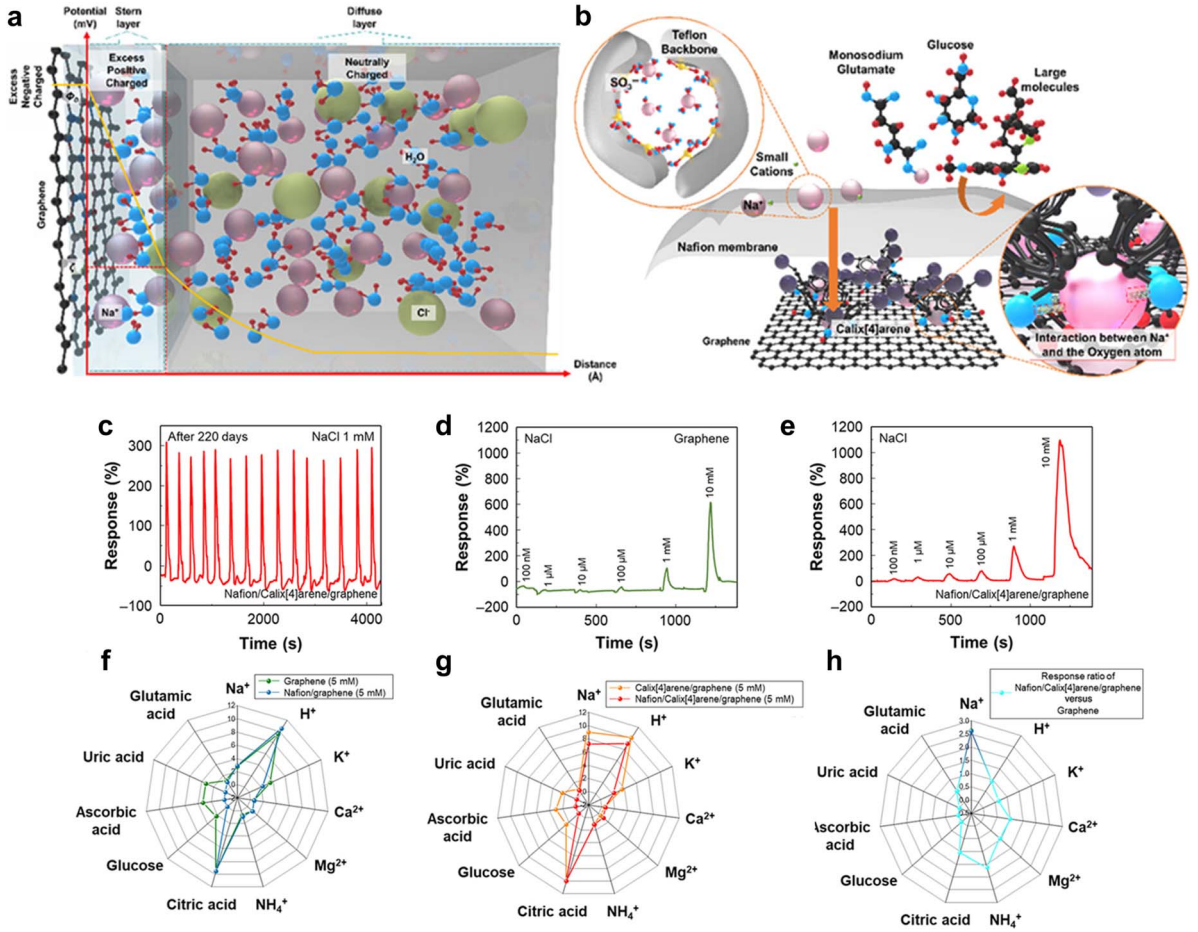

Fig. 8 Mechanism and performance evaluation of calix[4]arene/Nafion-decorated graphene devices for Na^+ detection. (a) and (b) Schematic of the Na^+ adsorption and detection processes, highlighting selective transport and specific interactions with calix[4]arene. (c) Long-term stability test showing consistent responses after 220 days. (d) and (e) Detection limit measurements demonstrating superior sensitivity of calix[4]arene/Nafion-decorated graphene compared to pristine graphene. (f–h) Response ratios and radar graphs verify the increased Na^+ selectivity. Reproduced with permission from ref. 12 Copyright 2023, Wiley-VCH.

responses to NaCl after 220 days. Nafion/calix[4]arene/graphene is more sensitive than pristine graphene throughout a broad concentration range (from 10 μM to 10 mM), according to the detection limit investigations (Fig. 8d and e). The radar plots in Fig. 8f–h further confirm the enhanced selectivity of the receptor for Na^+ compared to other ions.[12]

4.2. Selective taste sensors using receptors

Receptors are used by selective taste sensors to detect particular molecules related to flavor, while reducing interference from other substances. These sensors are made to detect target analytes with great accuracy and reliability. Receptor-based designs are used in selective taste sensors to reduce interference from other substances and provide high sensitivity for target analytes. Accurately identifying taste-related chemicals in complicated mixtures requires the use of these technologies. Fig. 9 demonstrates a colorimetric and ratiometric glucose detection system based on the pH-sensitive conformational switch of i-motif DNA.[87,88] Glucose oxidase (GO_x) induces the oxidation of glucose to produce gluconic acid and H^+ ions, as shown in the schematic in Fig. 9a. These H^+ ions cause the i-motif DNA (Poly(24C)) to fold, modifying how it interacts with methylene blue (MB) and producing a detectable colorimetric reaction.[89,90] Fig. 9b illustrates the selectivity of this device, demonstrating that the sensor responds selectively to glucose, while demonstrating very little interference from other molecules such as fructose and ascorbic acid. Even in complicated mixtures, this great selectivity guarantees accurate glucose detection. As shown in Fig. 9c, the stability of the sensor was assessed over a seven-day period using a glucose solution containing 800 μmol L^{-1}. The long-term reliability of the sensor for practical uses is confirmed by its consistent color responses during this period. Fig. 9d presents the UV-vis spectra of the Poly(24C)-MB system, which exhibit obvious differences in absorbance ratios from 5 to 800 μmol L^{-1} as the glucose concentration increases. With an excellent correlation coefficient ($R^2 = 0.997$), the calibration curve in Fig. 9e shows a linear relationship between the absorbance ratio ($A_{664\ nm}/A_{538\ nm}$) and glucose concentration. This linearity demonstrates the high precision and reliability of the sensor for quantitative glucose detection.[24]

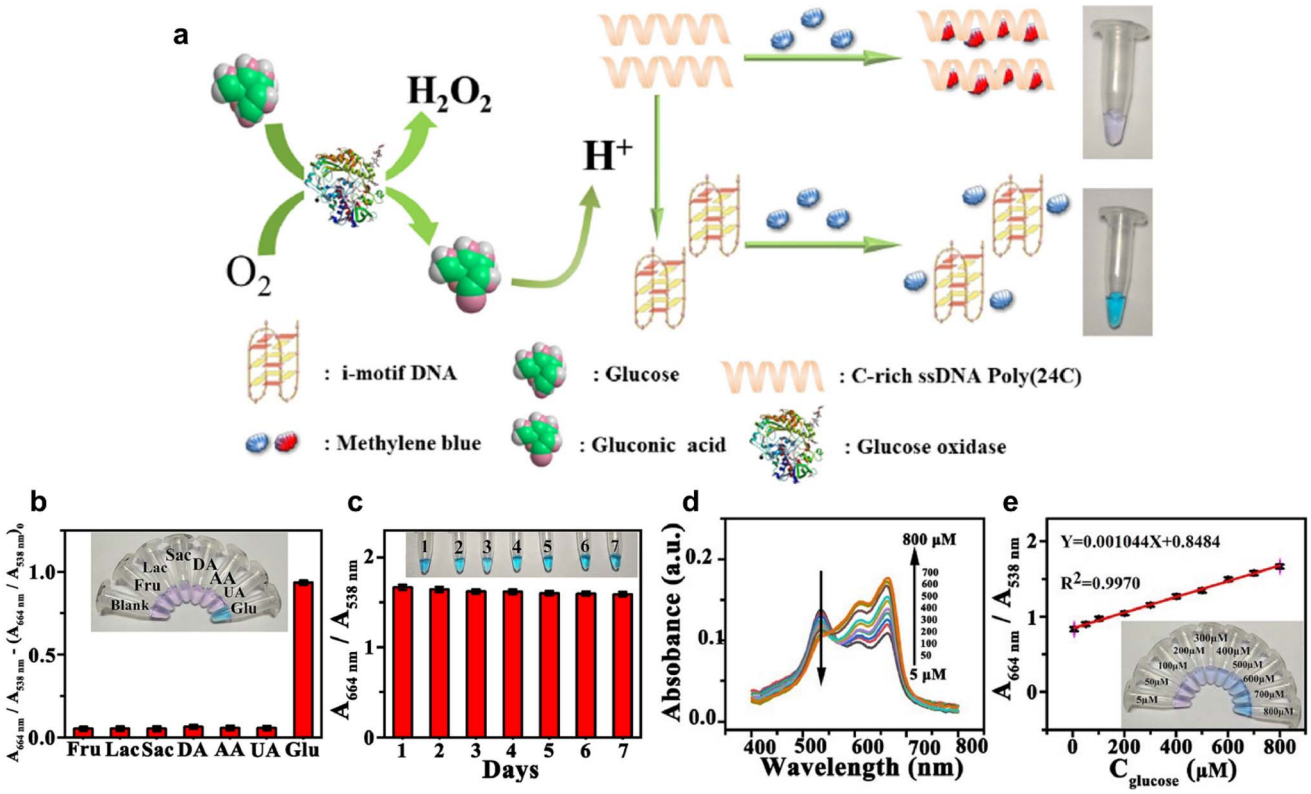

Fig. 9 Colorimetric and ratiometric glucose detection based on pH-sensitive i-motif DNA. (a) Schematic of glucose detection mechanism using GO_x and i-motif DNA (Poly(24C)). (b) Selectivity test for glucose against interferents. (c) Sensor stability over seven days. (d) and (e) UV-vis spectra and calibration curve demonstrating linear response to glucose concentrations ($R^2 = 0.997$). Reproduced with permission from ref. 24 Copyright 2020, Elsevier.

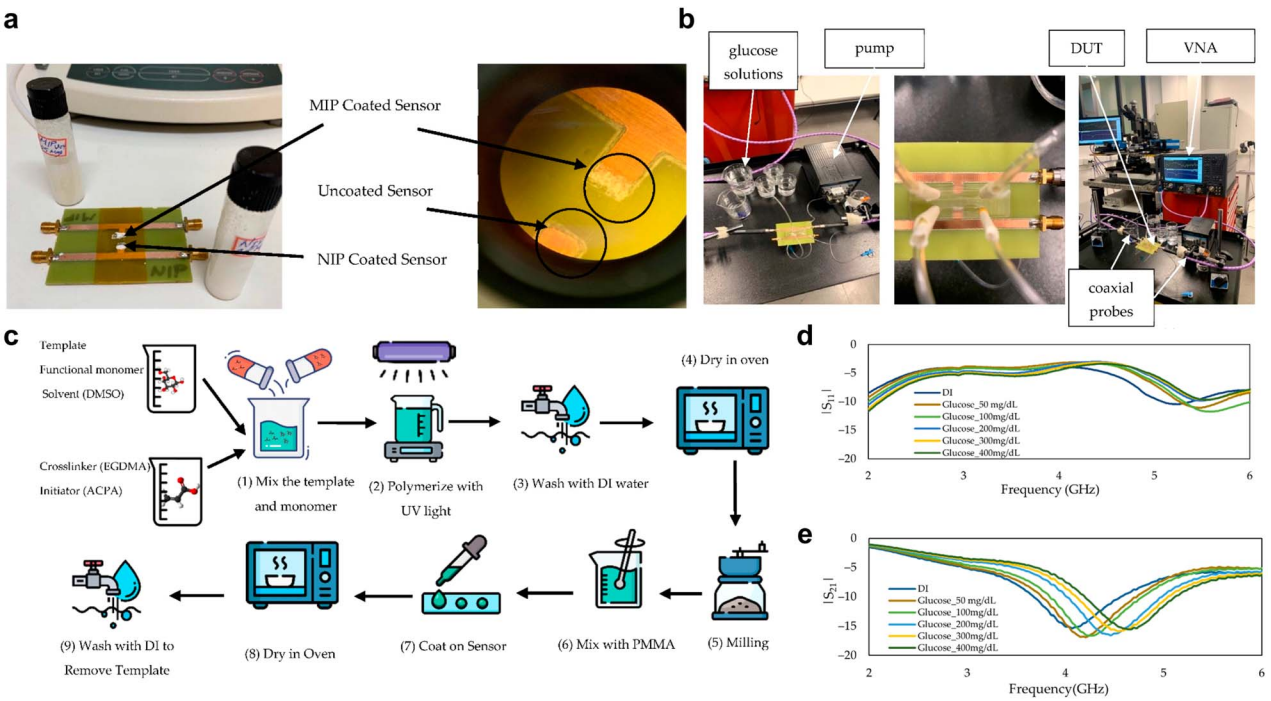

Fig. 10 Fabrication and performance of MIP-coated microwave-based stub biosensors for glucose detection. (a) and (b) Fabricated biosensors and experimental testing setup. (c) Schematic of sensor preparation with MIP. (d) and (e) Frequency response curves showing sensitivity to varying glucose concentrations. Reproduced with permission from ref. 27 Copyright 2022, MDPI.

Fig. 10 illustrates an MIP-coated microwave-based stub biosensor for selective glucose detection. An image of the constructed biosensor is displayed in Fig. 10a, featuring stub resonators coated with MIP and non-imprinted polymer (NIP). A peristaltic pump for solution flow, coaxial probes and a vector network analyzer (VNA) for accurate sensor response measurement make up the experimental setup, which is shown in Fig. 10b. Fig. 10c shows a schematic representation of the fabrication process, in which MIP is applied to stub resonators to provide selective binding sites that are especially suited for glucose molecules. The sensitivity and selectivity of the biosensor are improved by this receptor-based design. The frequency response curves in Fig. 10d demonstrate variations in the reflection coefficient (S_{11}) with different glucose concentrations (50–400 mg dL^{-1}), highlighting the ability of the sensor to detect changes in glucose concentration accurately. Similarly, the transmission coefficient (S_{21}) curves in Fig. 10e further confirm the superior sensitivity of the MIP-coated sensors compared to the NIP-coated sensors, proving their reliability for practical applications.[27] The basic components of E-tongue systems are receptors, which imitate biological recognition mechanisms to allow the accurate and selective detection of target analytes. These receptors are carefully engineered to improve the sensitivity and selectivity, ensuring reliable functioning even in complex mixtures. Receptor-based sensors are highly accurate at detecting ions, glucose and other biomolecules by promoting particular chemical interactions.[91,92]

5. E-tongue

This section explores several types of sensor arrays commonly used for detecting chemical or biological analytes, with a focus on pH sensor arrays, ISFET systems and triboelectric sensor arrays. While careful engineering of the physical sensor setup is critical, data processing methods can be just as decisive in determining its overall performance. In many cases, signal features are extracted, and then fed into machine-learning (ML) or other pattern-recognition approaches, enabling a more

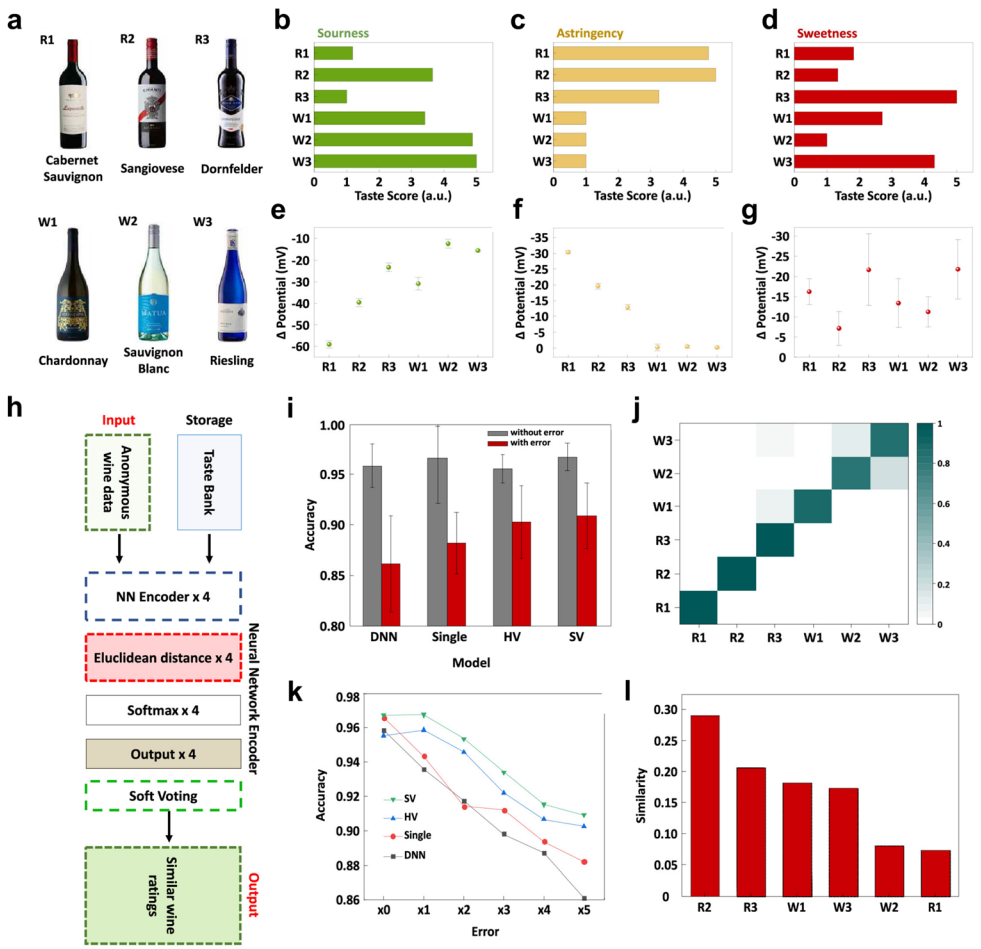

Fig. 11 (a) Selection of six different wines for classification analysis based on grape varietals: Cabernet Sauvignon (R1), Sangiovese (R2), Dornfelder (R3), Chardonnay (W1), Sauvignon Blanc (W2), and Riesling (W3). (b–d) Normalized taste values of six wines data from online user reviews with respect to the sourness (b), astringency (c) and sweetness (d). (e–g) Potential responses of the six wines for sourness (e), astringency (f) and sweetness (g) using the taste sensors of the artificial E-tongue system. (h) Pipeline for anonymous wine data classification. (i) Comparison of classification test accuracy of four models (DNN, single prototype based network, hard voting and soft voting) for data with and without errors. (j) Confusion matrix for six types of wine. (k) Accuracy comparison between four models with different numbers of errors. (l) Similarity rating between trained wine data and anonymous wine data. Reproduced with permission from ref. 94 Copyright 2023, the American Chemical Society.

accurate, robust classification.[93] Notably, research on ML adaptation in E-tongue arrays is currently ongoing, with continued efforts to refine algorithms and data-handling techniques.

A recent study by Jang *et al.* developed a "taste bud-inspired" sensor array to evaluate multiple flavors from a single drop of liquid.[94] For classification, data on six different wines with distinct taste profiles were gathered, as shown in Fig. 11a–d. By coupling lipid-membrane-based electrodes with an optimized deep-learning model, the system converts raw electrical signals into interpretable "taste profiles", as shown in Fig. 11e–g, which are then labeled and compiled into a "data bank." Next, the signals of an "unknown" wine go into four parallel neural networks (Fig. 11h), each mapping the input to an embedded vector space for prototype-based classification (Fig. 11i). Each network outputs a predicted wine type (Fig. 11j), and after accuracy comparison (Fig. 11k), those predictions are combined into a final classification or a "similarity" ranking with known wines in the data bank (Fig. 11l). By employing bootstrap-based data augmentation and prototype-based classifiers, high classification accuracy was maintained, even when a notable fraction of the sensor data contained errors. A combined hardware–software approach using specialized sensor arrays and advanced data processing may provide rapid, precise and multiparameter detection.

5.1. pH sensor arrays

A pH sensor array consists of multiple miniaturized pH-sensing units arranged on a shared substrate. Each unit responds to changes in acidity or basicity through interactions between ion-sensitive materials and the analyte of interest. By including several individually addressable sensing spots in one device, arrays can capture spatial variations in pH and allow the cross-validation of measurements, thereby enhancing the overall reliability. Some modern pH sensor arrays integrate flexible substrates such as polymeric films or paper to improve the adaptability in applications such as wound monitoring and wearable diagnostics. The choice of functional materials is diverse, ranging from conductive polymers to inorganic films or hybrid membranes. When well-designed, these arrays typically exhibit high sensitivity, rapid response and good stability over a broad pH range, and they can be further customized to minimize interference from other ions or environmental factors.

Iridium oxide (IrO_x) sensor arrays are well-suited for pH detection because of their excellent stability, durability, low temperature sensitivity, biocompatibility, ease of fabrication, low cross-sensitivity to interfering ions and broad pH operational range.

Nguyen *et al.* developed a 4 × 4 pH sensor array comprised of IrO_x WE paired with Ag/AgCl RE, all integrated on a polyimide film.[95] The design leverages the sol–gel deposition of IrO_x, followed by moderate thermal processing at 300 °C, which is compatible with flexible polymers. Each sensing cell can be individually addressed for multichannel readout. Tests across a 2–12 pH span showed Nernstian potential responses in the range of 57.0–63.4 mV pH^{-1}, minimal drift and robust repeatability. The response times were in the order of a few seconds to reach stable output, enabling its use in continuous or real-time measurements.

In addition, mechanical flexibility studies demonstrated that the sensor array maintains a reliable performance up to certain bending radii, underlining its potential for wearable or biomedical applications requiring conformal contact with soft tissues or curved surfaces. Focusing on ion-interference issues in environments that contain both H^+ and Na^+, Yang *et al.* introduced a flexible iridium IrO_x sensor array featuring parallel measurement channels.[96] An IrO_x electrode was devoted to pH sensing, while a second IrO_x electrode coated with a sodium-selective membrane monitored the Na^+ concentration. By simultaneously measuring the pH and Na^+ levels, the device compensated for voltage drifts caused by varying Na^+ concentrations, thereby calibrating the pH readings in real time. The pH-sensitive channel achieved a sensitivity of 61.46 mV pH^{-1} in the pH range from acid to alkaline measured at room temperature, while the Na^+ channel captured potential shifts in response to different Na^+ levels. This dual-measurement strategy significantly improved the pH accuracy in ion-rich environments, a critical advantage in applications ranging from water-quality monitoring to physiological fluid analysis and process control.

PANI-based sensor arrays offer an effective combination of strong pH sensitivity, low fabrication cost and biocompatibility for diverse detection needs. Rahimi *et al.* presented a screen-printed pH sensor array on a polymer-coated commercial paper substrate, aiming to provide an affordable and disposable tool for monitoring wound health.[97] Each sensing unit features two electrodes, a carbon WE coated with a proton-sensitive PANI membrane and a miniaturized Ag/AgCl RE. Laser micromachining was used to create both the sensing areas and self-aligned passivation layers. The array demonstrated a linear response with r^2 value of 0.9734, over the pH range of 4–10 with an average sensitivity of about −50 mV pH^{-1}. Real-time measurements revealed a rise time of 12 s and a fall time of 36 s for a pH transition from 8 → 6 → 8, indicating comparatively rapid adaptation when the sample acidity changes. Practical aspects such as potential biofouling and skin conformity are mitigated by the paper-based design, which is both flexible and lightweight. Additionally, biocompatibility tests with human keratinocytes confirmed the minimal cytotoxic effects, highlighting the potential of this sensor for *in situ* wound monitoring and other biomedical applications. Lee *et al.* developed a soft, conformable microneedle pH sensor array to measure dermal acidity and map tissue damage in peripheral artery disease (PAD).[31] Fig. 12a presents a schematic overview of the device, which integrates epoxy siloxane microneedles and a PDMS substrate for both mechanical robustness and conformal contact. As seen in Fig. 12b, the microneedles can be flexed and inserted repeatedly without significant structural damage. Fig. 12c shows an SEM micrograph of an individual microneedle featuring a PANI coating to enhance the pH sensitivity. Meanwhile, Fig. 12d and e reveal a 5 × 5 sensor layout and a 3D topographical scan, respectively, underscoring

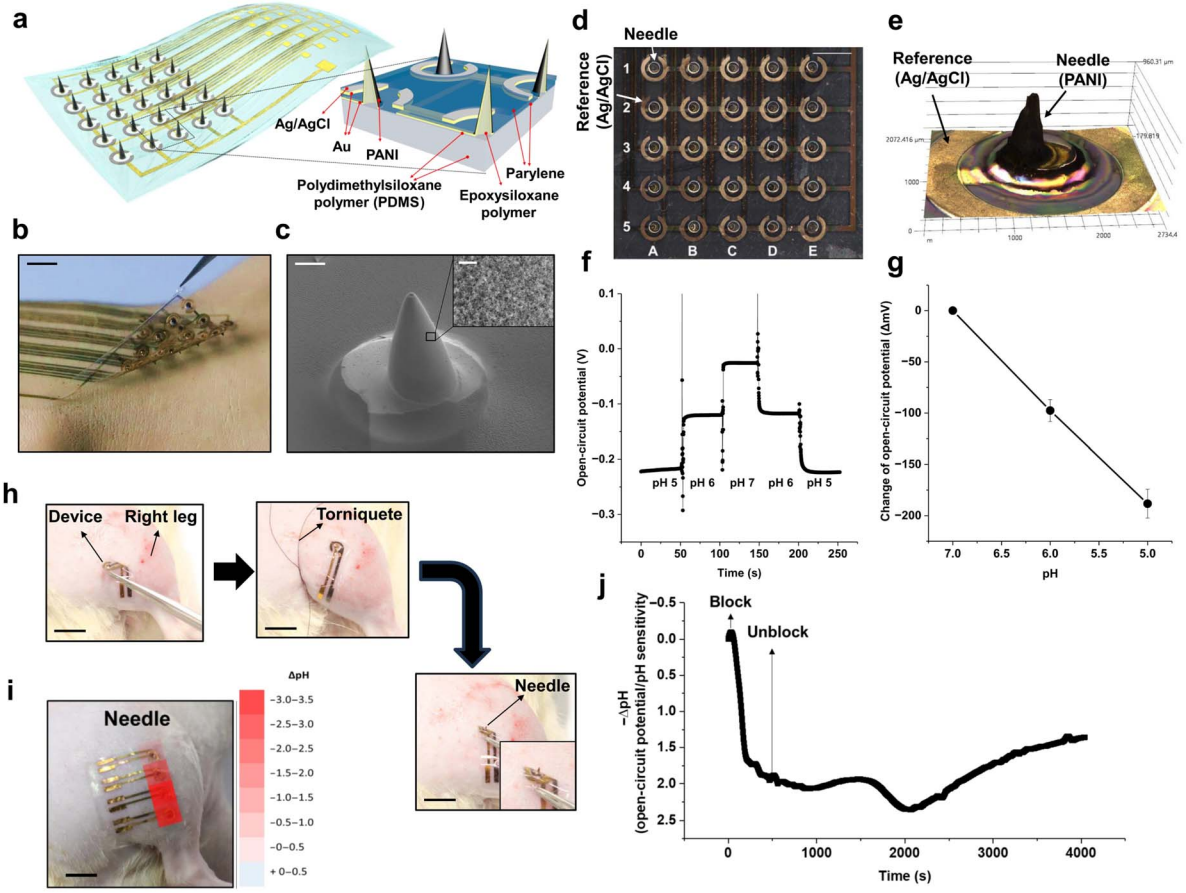

Fig. 12 (a) Overall scheme of a flexible pH sensor array with microneedles. Inset: cross section of device. (b) 5 × 5 pH sensor array with microneedles. Scale bar, 5 mm. (c) SEM image of a microneedle. Scale bar, 250 μm. Inset: image of polyamine deposited on a microneedle. Scale bar, 5 μm. (d) Microscope image of 5 × 5 pH sensor array. Scale bar, 5 mm. (e) 3D microscope image of a microneedle. (f) OCP time curve of a single pH sensor with pH change. (g) Change in OCP of 25 pH sensors. (h) Photo of setting of a single flexible pH sensor on a rat with vascular blockage. Scale bars, 10 mm. (i) Photograph showing location and pH distribution with microneedle type sensors. Scale bars, 10 mm. (j) Recorded change of OCP of a pH sensor with microneedles. Reproduced with permission from ref. 31 Copyright 2021, AAAS.

the uniform needle geometry and RE placement. By electrochemically tracking OCP, the sensor exhibited a linear pH response (illustrated in Fig. 12f and g) with high pH sensitivity. To evaluate its clinical relevance, Fig. 12h–j detail the application of the device to a rat model of PAD, where a tourniquet-induced ischemic region triggers local acidosis, which is captured by the microneedle array as variations in pH. By evaluating elastic materials, miniaturized architectures and durable microneedle designs, current studies on pH sensor arrays demonstrate a pathway toward developing portable, wearable sensor platforms that offer high performance chemical detection. Nevertheless, they also face practical challenges. They typically require periodic calibration to maintain accuracy, especially when exposed to complex matrices with strong buffering capacities or high ionic strengths. Biofouling, drift and signal instability may also limit their long-term usage, necessitating careful selection of materials and protective coatings.[98] Despite these hurdles, the rapid evolution of fabrication and surface-functionalization strategies has led to increasingly robust and sensitive pH sensor arrays. As a result, these arrays continue to play a pivotal role in E-tongue technologies, facilitating precise monitoring in a wide spectrum of real-world applications.

5.2. ISFET arrays

ISFETs have emerged as a promising platform for E-tongue technologies due to their inherent ability to transduce chemical stimuli into direct electrical signals. In an ISFET, the conventional MOSFET gate is replaced by an ISM or dielectric layer, where the electrostatic interactions between the analyte ions and the sensor surface induce a measurable shift in the threshold voltage. By arranging multiple ISFETs, each functionalized for distinct ionic or molecular targets, into a single array, it becomes possible to detect and differentiate taste profiles simultaneously. This multichannel detection strategy not only enhances the selectivity and sensitivity of taste-related measurements, but also enables rapid, label-free and miniaturized analysis. Moreover, the fabrication of ISFET arrays can leverage established semiconductor processing protocols, facilitating device integration, cost-effective mass production

and scalable designs. Consequently, ISFET-based E-tongues have proven advantageous for a broad range of applications, including quality control in the food and beverage industry, environmental monitoring and clinical diagnostics.

Moser *et al.* presented a systematic study on enhancing the sensing performance of CMOS-based ISFET arrays by successively removing the passivation layers through reactive ion etching (RIE).[99] In standard unmodified CMOS, multi-layer passivation, commonly comprising polyimide, silicon nitride and silicon dioxide, tends to attenuate pH signals, trap charges and introduce drift and noise. By precisely tuning the RIE parameters such as plasma pressure, gas flow and power, selective, material-specific etch steps that expose or thin the top nitride and oxide layers were achieved. As a result, their 4000-pixel ISFET array demonstrated higher pH sensitivity, reduced threshold voltage offset and significantly improved SNR. Notably, up to an 80% reduction in offset variability and a 40 dB increase in SNR compared to the devices with non-etched passivation were reported.

Honda and co-workers focused on a flexible and detachable ISFET-based pH sensor array that addresses key challenges in large-area sensing, particularly mechanical flexibility, reusability and cost efficiency.[100] A two-part system consisting of a reusable transistor sheet featuring InGaZnO-based ISFETs and a disposable pH-sensitive membrane sheet, electrically coupled *via* a soft, stretchable Ag electrode was proposed. This design preserves mechanical compliance, allowing it to conform to curved or irregular surfaces without compromising electrical contact. Through systematic testing, good stability was shown over multiple attach/detach cycles and bending radii, with a measured pH sensitivity of around 66.5 mV pH^{-1}.

Fakih and coauthors presented a wafer-scale graphene sensor array capable of resolving multiple ionic species in real time.[29] Fig. 13a outlines the basic setup, wherein an RE and a graphene FET are immersed in an electrolytic solution. As illustrated in Fig. 13b and c, a tailored ion-selective membrane ensures that the target ion concentration is effectively buffered, inducing a measurable shift in the Fermi level of graphene. By incorporating distinct ionophore membranes for K^+, Na^+, NH^{4+}, NO^{3-}, $SO_4{}^{2-}$, $HPO_4{}^{2-}$ and Cl^- onto separate transistors, the device simultaneously tracks multiple ions, even in complex solution matrices. As demonstrated in Fig. 13d and e, an

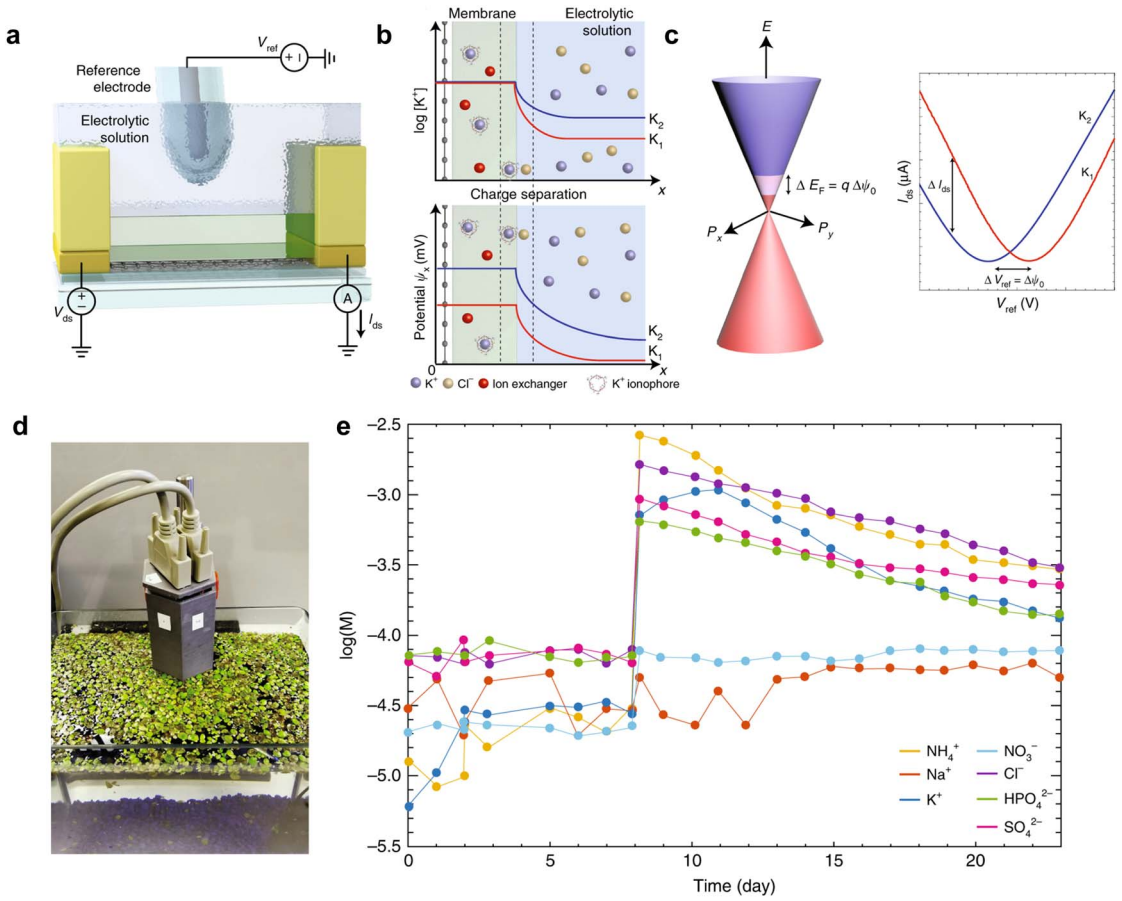

Fig. 13 (a) Schematic of the electrical setup for monitoring the drain current (I_{ds}) through a graphene channel under varying RE potentials (V_{ref}) at a constant bias voltage (V_{ds}). (b) Illustration of ion separation at the membrane/electrolyte interface, generating a surface potential influenced by analyte concentration. (c) Surface potential shifts modulate the graphene Fermi level, altering the ISFET transfer curve. (d) Optical image of the ISFET array deployed in an aquarium with duckweed. (e) Temporal ion concentration profiles in the aquarium, calculated using Nikolskii–Eisenman equations. Salt nutrients were added on day 8 to support plant growth. Reproduced with permission from ref. 29 Copyright 2020, Springer Nature.

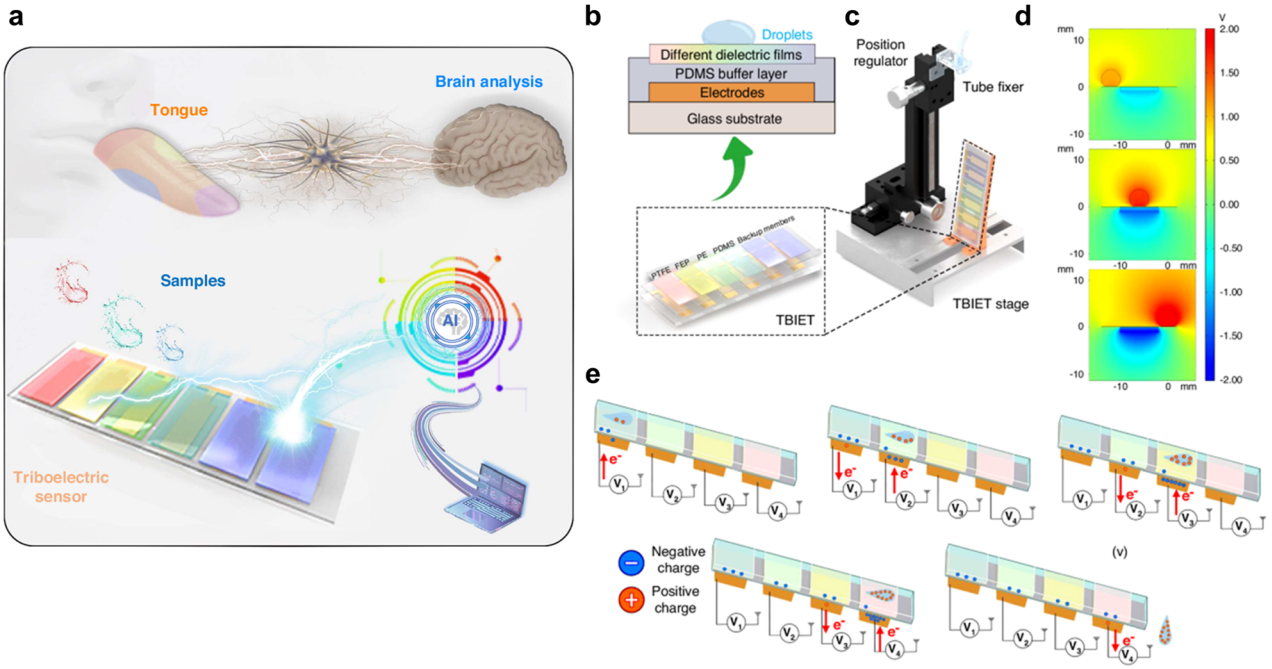

Fig. 14 Conceptual design, structure and working mechanism of the TBIET device. (a) Conceptual illustration of the TBIET device integrated with AI for droplet detection and data analysis. The system mimics human taste perception through a triboelectric sensor array, which processes chemical information from droplets and translates it into digital signals for brain-inspired analysis. (b) Structural schematic of the TBIET device, showing its four-layer configuration: glass substrate, electrode layer, PDMS buffer layer and various dielectric films. The three-dimensional representation highlights the compact design of the device for efficient droplet sensing. (c) Position-adjustable support stage designed to fix the TBIET device and the dropper tube. This setup ensures precise alignment of droplets with the sensor array during operation. (d) Simulated potential distribution across the electrodes and droplets using COMSOL Multiphysics. The color gradient illustrates the electric potential variations induced by droplet interactions with the triboelectric layers, providing insight into the charge transfer mechanisms. (e) Working principle of the TBIET device: as droplets interact with different dielectric films, triboelectric charges are generated and transferred to adjacent electrodes. This sequential charge transfer creates distinct voltage outputs, enabling the identification and classification of chemical components within the droplets. Reproduced with permission from ref. 32 Copyright 2024, Springer Nature.

extended test in an aquarium with *lemnoideae lemna* revealed discernible changes in ionic concentrations during nutrient uptake by the plants.

Recent developments in ISFET-based E-tongues have substantially enhanced their sensitivity, selectivity and mechanical robustness. However, key challenges persist in ensuring their long-term stability under repeated mechanical stress, mitigating noise, managing consistent calibration for multi-ion detection and streamlining large-scale manufacturing. Moving forward, integrating advanced data-

Table 2 SWOT analysis of ISFET-based and triboelectric-based E-tongues

	ISFET	Triboelectric
Strengths	High sensitivity and fast response CMOS compatible Supports surface chemistries (enzymes and aptamers) Capable of real-time, continuous monitoring	Self-powered Simple fabrication Suitable for disposable sensing platforms
Weaknesses	Frequent calibration demanded Use of silicon and metal oxides increases environmental impact during fabrication External power required	Lower selectivity and quantification accuracy Limited standardization and maturity
Opportunities	Integration with sustainable electronics Multiplexed sensing in agricultural runoff or food production for environmental monitoring	Deployment in resource-limited settings due to low-cost, battery-free operation Development of fully biodegradable, disposable sensors for single use food or water quality tests
Threats	Increasing demand for low-power and disposable systems may favor alternative sensor technologies Environmental and cost concerns related to semiconductor manufacturing and e-waste	Lack of international standards may slow regulatory approval and scalability

Table 3 Comparative summary of sensing materials, platforms and their performance characteristics

Channel material	Platform	Target	Detection range	Measurement method	Reference
Fluorinated graphene	ISFET	Na^+	0.1 mM–1 M	Transfer curves, amperometric	34
Ag NPs/GO	Potentiometric	Na^+	0–100 mM	Cyclic voltammograms	38
MoS_2–PANI	Potentiometric	pH	4–8 pH	Cyclic voltammograms	40
$Ni_3(HITP)_2$	ISFET	Gluconic acid	1 μg mL^{-1}–1 mg mL^{-1}	Transfer curves	20
Nafion/Ti_3C_2	ISFET	pH	5.63–8.11 pH	Amperometric	11
Au-Decorated graphene	ISFET	Glucose	0.01–10 mM	Transfer curves, on–off available sensing curves	10
Au-Decorated graphene	ISFET	pH	5.55–8.05 pH	Transfer curves, on-off available sensing curves	12
Poly(24C)-MB	Colorimetric	Glucose	5–800 μM	UV spectra	24
Glucose-MIP (AA/EGDMA)	Microwave resonator	Glucose	50–400 mg dL^{-1}	Resonant frequency shift	27
TDAB, 1-hexadecanol for KCl	Lipid membrane	KCl, tartaric acid, tannic acid, sucrose	0.05–5.0 wt% KCl	Open-circuit potential	94
TOMA, OA, BP for tartaric acid			0.01–1.0 wt% tartaric acid		
TDAB for tannic acid			0.01–1.0 wt% tannic acid		
TDAB, trimellitic acid for sucrose			1 mM to 1 M sucrose		
PANI on Au	Potentiometric (5 × 5 array)	pH	3–7 pH	Open-circuit potential	31
Graphene	ISFET (array)	Na^+	1 μM–31 mM	Transfer curves, amperometric	29
PTFE, FEP, PE	Triboelectric (4-channel array)	Na^+	0.05–5.4 mol L^{-1}	Triboelectric voltage measurement with LDA, SVM, RF algorithms	32

processing methods, exploring new receptor chemistries and incorporating 3D-printed or microfluidic systems may further refine E-tongue capabilities. Continued research along these lines promises to broaden the adoption of ISFET-based sensor arrays for various applications.

5.3. Triboelectric sensor arrays

Triboelectric sensor arrays leverage the charge generated by contact or friction between specialized layers and liquid samples to classify and quantify taste components.[32] In these systems, droplets flowing or impacting onto triboelectric materials induce measurable voltage or current signals that reflect the ion content, pH and viscosity of the sample. Crucially, this charge transfer occurs spontaneously, allowing operation without external power sources.[101] By combining multiple triboelectric sensing channels, each tailored with different material or structural properties, the system captures distinctive electrical fingerprints for diverse liquids. These self-powered, low-cost platforms are well suited for on-site, real-time taste sensing in diverse applications ranging from food quality control to environmental testing.

Liu *et al.* proposed a triboelectric bionic E-tongue (TBIET) that utilizes multiple dielectric films, electrodes and a polymer buffer layer assembled on a single chip for droplet classification *via* self-generated electrical signals.[32] Fig. 14a provides an overview of the biomimetic framework, drawing parallels to how human tongues interface with the brain for taste perception. In this design, droplets traverse a surface composed of multiple sensing channels, each exhibiting distinct triboelectric properties. Fig. 14b and c depict the device structure, wherein the channels are mounted on a glass substrate and shielded by a PDMS buffer layer to facilitate triboelectric effects. As the droplets move across the dielectric films, solid–liquid contact initiates charge transfer, yielding unique voltage responses (illustrated by the color-mapped plots in Fig. 14d). The underlying mechanism of electrons transferring between the film surfaces and the droplets is further elucidated in Fig. 14e. These voltage signals, once processed through a trained AI model, enable the TBIET to accurately discriminate among various chemical, environmental and food samples, offering a compact and self-sustained platform for on-site liquid analysis.

In a related advancement, Wei *et al.* presented a dual-sensory fusion triboelectric liquid-sensing system that combines droplet-based triboelectric signals with real-time imagery of the same droplets.[2] By embedding two spatially arranged electrodes on a hydrophobic film, the device generated distinct voltage waveforms as droplets of different liquids contacting and sliding down the film, reflecting the ion content and viscosity of each fluid. At the same time, a camera captured key visual features such as color, shape and sliding speed, which further characterized the sample. A convolutional neural network integrated both triboelectric and visual inputs to achieve highly accurate classification of multiple liquids, ranging from vinegar and liquor to coffee and water. In test scenarios involving robotic taste emulation, environmental pH monitoring and food analysis, the recognition accuracies consistently exceeded 90% and rose to as high as 96% with the combined data

channels. Because the triboelectric signals are self-generated (no external power is required) and the optical element is relatively simple, the platform highlights the potential of affordable, multifunctional and AI-enabled sensing for real-time liquid quality control.

Zhao *et al.* designed a self-powered flexible sour sensor that detects ascorbic acid (AA) concentrations by coupling triboelectrification with an enzymatic reaction.[102] Essentially, they patterned a polypyrrole/PDMS film onto a copper mesh, and then immobilized ascorbate oxidase (AAO) on the polypyrrole surface. As a droplet containing AA is placed on the film, the enzymatic reaction alters the local proton concentration, shifting the charge-transfer dynamics when the substrate flexes. In other words, the triboelectric current the device generates upon deformation is inversely proportional to the AA concentration in the sample. Additionally, since ordinary mechanical bending suffices to produce a measurable current signal, no external power is required. The experimental results showed strong linearity and sensitivity across a wide ascorbic acid range, and the authors further demonstrated the real-world feasibility by analyzing commercial beverages. Altogether, this enzyme-modified triboelectric scheme extends taste detection to sourness and highlights the potential for wearable, low-cost triboelectric tongues that rely on built-in bioreactions to classify food or drink quality on the fly.

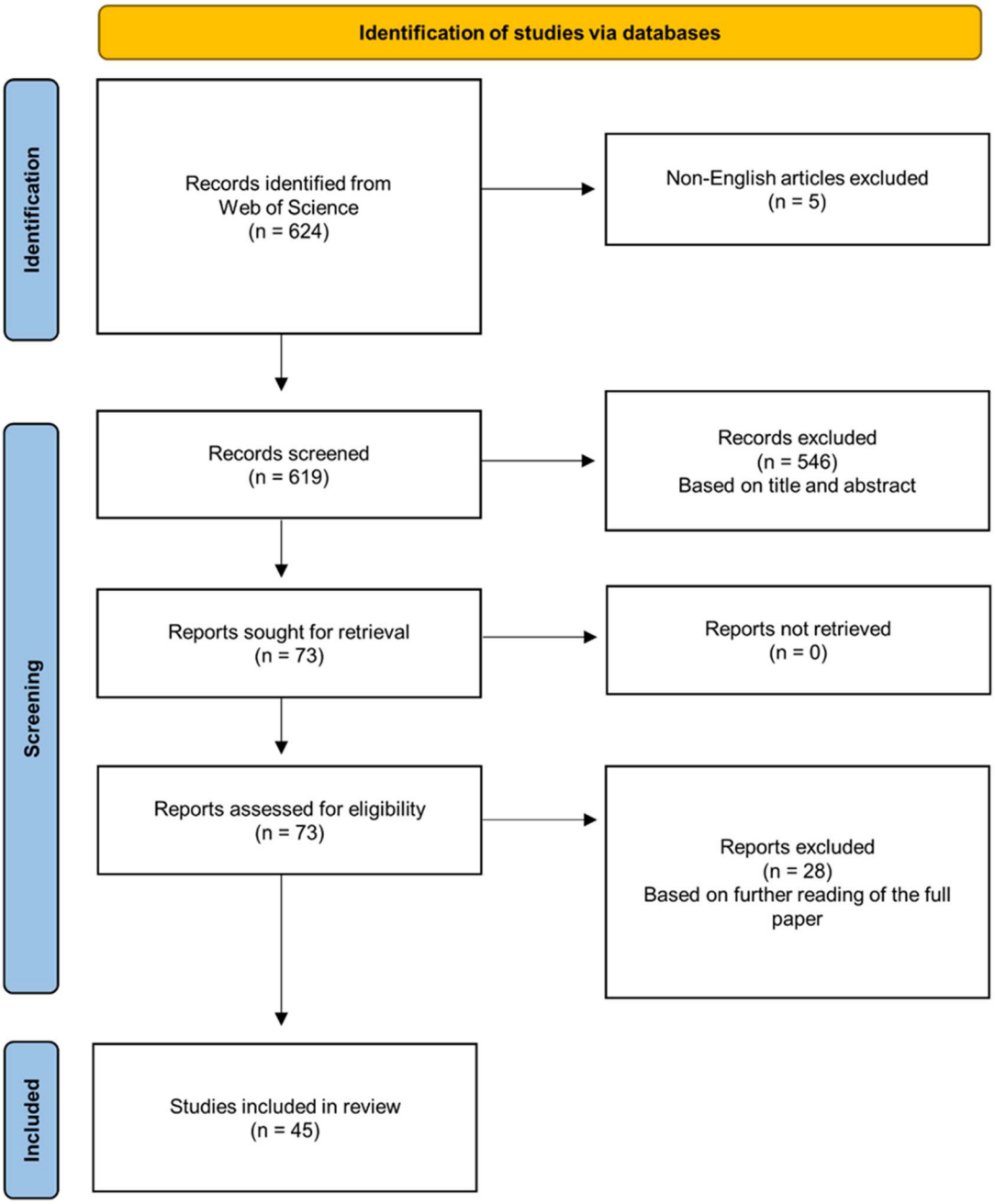

Fig. 15 PRISMA diagram illustrating the exclusion process based on the scope of the narrative review.

Triboelectric tongue arrays enable rapid, self-powered taste sensing using microliters of liquid, offering cost-effective classification through optimized polymer films and advanced data analysis.[2,102] However, although promising, they still face challenges in stability, droplet handling and standardized protocols. Thus, to provide a comparative perspective on the diversity of sensor architectures in E-tongue systems, a SWOT (Strengths, Weaknesses, Opportunities and Threats) analysis of ISFET- and triboelectric-based sensors is presented in Table 2. ISFET arrays offer high sensitivity, fast response and CMOS compatibility, making them ideal for real-time, multiplexed sensing.[29,99] However, their reliance on silicon and external power limits their sustainability and scalability.[32] In contrast, triboelectric sensors are self-powered and low-cost, features that align well with eco-friendly, disposable or off-grid applications, although they currently face challenges in selectivity and standardization.[32] These complementary strengths suggest a path forward through hybrid systems that merge the analytical performance of ISFETs with the sustainability of triboelectric designs (Table 3).

6. Materials and methods

The literature search was conducted using the Web of Science database with a publication date range from 2005 to 2025, resulting in an initial yield of 624 peer-reviewed journal articles identified through manual curation. After screening based on titles, abstracts and full-text, 45 articles were selected for inclusion, as illustrated in Fig. 15. Although this review adopts a narrative approach, the literature search was conducted systematically to ensure comprehensive coverage of relevant studies. Each selected article was critically reviewed by the authors to extract and synthesize key findings. While this review does not include a formal systematic review protocol, meta-analysis or risk of bias assessment, it aims to provide a transparent and rigorous narrative synthesis of the current state of research.

7. Conclusions

The escalating demand for rapid, high fidelity taste detection has made the robust screening of taste components a critical challenge. This review provides outlines on how recent advancements in active channels, molecular sieves, receptors and sensor arrays enhance the sensitivity, selectivity and real-world applicability of E-tongue systems. Integration of these elements yields synergistic effects, supporting applications from benchtop analysis to wearable diagnostics. However, despite the substantial progress, ongoing obstacles include cross-sensitivity and varying detection limits, necessitating careful sensor selection and robust calibration. E-tongue technologies not only improve the analytical performance but also advance sustainability by reducing the energy use, material waste and food loss *via* on-site detection. However, the environmental impacts associated with synthesizing and disposing of advanced nanomaterials, such as 2D materials and MOFs, require further evaluation through lifecycle assessment and green manufacturing. Looking ahead, integration with Internet of Things (IoT) devices and AI-driven data analytics is expected to improve real-time, multi-analyte sensing and address current limitations. For E-tongue technologies to transition from laboratory prototypes to regulatory-approved tools in food and clinical contexts, key issues such as measurement standardization, calibration management, system interoperability and user training must be addressed. Additionally, real-world deployment requires robust long-term stability, scalable manufacturing, cost-effectiveness and regulatory compliance. To guarantee general acceptance and trust among customers, collaboration with the industry and regulatory organizations will be essential. Progress in these areas will be essential for consistent, reliable and broadly accepted deployment. As E-tongue systems mature, their future success will depend equally on continued technical innovation and commitment to sustainable, responsible deployment across diverse real-world environments.

Author contributions

Hyuk Jin Kim: investigation, visualization, original draft preparation. Jun Uh Hyun: investigation, visualization, original draft preparation. Ho Won Jang: writing – reviewing and editing, supervision.

Conflicts of interest

There are no conflicts to declare.

Data availability

No primary research results, software or code has been included and no new data were generated or analysed as part of this review.

The list of reviewed articles is available as SI. See DOI: **https://doi.org/10.1039/d5fb00237k**.

Acknowledgements

This work was financially supported by the Nano Material Technology Development Program (RS-2022-NR068132 and RS-2024-00405016) through NRF (National Research Foundation of Korea), funded by the Ministry of Science and ICT. This research was also supported by the Research Institute of Advanced Materials (RIAM), Inter University Semiconductor Research Center (ISRC), SOFT Foundry Institute and Institute of Engineering Research at Seoul National University.

Notes and references

1 A. Riul, C. A. R. Dantas, C. M. Miyazaki and O. N. Oliveira, *Analyst*, 2010, **135**, 2481.
2 X. Wei, B. Wang, X. Cao, H. Zhou, Z. Wu and Z. L. Wang, *Nat. Food*, 2023, **4**, 721.
3 Y. Choi, S. Lee, S. Lee, S. Hong and H. W. Kwon, *ACS Sens.*, 2022, **7**, 3682.

4 T. Goto, S. Shimamoto, A. Ohtsuka and D. Ijiri, *Anim. Sci. J.*, 2021, **92**, e13510.
5 H. Ullah, A. S. Khan, B. Murtaza, A. Hichami and N. A. Khan, *Nutrients*, 2022, **14**, 197.
6 S. Zhao, H. Zheng, Y. Lu, N. Zhang, O. P. Soladoye, Y. Zhang and Y. Fu, *J. Agric. Food Chem.*, 2023, **71**, 13950.
7 M. C. Murillo-Cruz, N. Rodrigues, M. I. Dias, R. Bermejo-Román, A. C. A. Veloso, J. A. Pereira and A. M. Peres, *J. Am. Oil Chem. Soc.*, 2022, **99**, 1113.
8 M. del Valle, *Int. J. Electrochem.*, 2012, **2012**, 11.
9 B. Aouadi, J. L. Z. Zaukuu, F. Vitális, Z. Bodor, O. Fehér, Z. Gillay, G. Bazar and Z. Kovacs, *Sensors*, 2020, **20**, 5479.
10 C. W. Lee, J. M. Suh, S. Choi, S. E. Jun, T. H. Lee, J. W. Yang, S. A. Lee, B. R. Lee, D. Yoo, S. Y. Kim, D. S. Kim and H. W. Jang, *npj 2D Mater. Appl.*, 2021, **5**, 39.
11 H. J. Kim, C. W. Lee, S. S. H. Park, S. Choi, S. S. H. Park, G. B. Nam, J. El Ryu, T. H. Eom, B. Kim, C. J. Kim, S. Y. Kim and H. W. Jang, *Sens. Actuators, B*, 2024, **409**, 135636.
12 C. W. Lee, S. E. Jun, S. J. Kim, T. H. Lee, S. A. Lee, J. W. Yang, J. H. Cho, S. Choi, C. joo Kim, S. Y. Kim and H. W. Jang, *InfoMat*, 2023, **5**, 7.
13 M. Otto and J. D. R. Thomas, *Anal. Chem.*, 1985, **57**, 2647.
14 P. Ciosek and W. Wróblewski, *Sensors*, 2011, **11**, 4688.
15 R. X. He, P. Lin, Z. K. Liu, H. W. Zhu, X. Z. Zhao, H. L. W. Chan and F. Yan, *Nano Lett.*, 2012, **12**, 3.
16 C. W. Lee, J. M. Suh and H. W. Jang, *Front. Chem.*, 2019, **7**, 708.
17 A. Pannone, A. Raj, H. Ravichandran, S. Das, Z. Chen, C. A. Price, M. Sultana and S. Das, *Nature*, 2024, **634**, 572.
18 S. S. Kaye, A. Dailly, O. M. Yaghi and J. R. Long, *J. Am. Chem. Soc.*, 2007, **129**, 14176.
19 X. Kang, X. Han, C. Yuan, C. Cheng, Y. Liu and Y. Cui, *J. Am. Chem. Soc.*, 2020, **142**, 16346.
20 B. Wang, Y. Luo, B. Liu and G. Duan, *ACS Appl. Mater. Interfaces*, 2019, **11**, 35935.
21 M. Radjabian and V. Abetz, *Prog. Polym. Sci.*, 2020, **102**, 101219.
22 J. Preat, D. Zanuy, J. Torras and C. Alema, *J. Phys. Chem. B*, 2009, **113**(24), 8284.
23 G. Wu, N. Zhang, A. Matarasso, I. Heck, H. Li, W. Lu, J. G. Phaup, M. J. Schneider, Y. Wu, Z. Weng, H. Sun, Z. Gao, X. Zhang, S. G. Sandberg, D. Parvin, E. Seaholm, S. K. Islam, X. Wang, P. E. M. Phillips, D. C. Castro, S. Ding, D. P. Li, M. R. Bruchas and Y. Zhang, *Nano Lett.*, 2022, **22**, 3668.
24 Q. Wang, T. Dai, P. Sun, X. Wang and G. Wang, *Talanta Open*, 2020, **1**, 100001.
25 Z. Jarolímová, M. Vishe, J. Lacour and E. Bakker, *Chem. Sci.*, 2016, **7**, 525.
26 M. J. Marsella, P. J. Carroll, T. M. Swager and R. J. Newland, *J. Am. Chem. Soc.*, 1995, **117**, 9842.
27 A. H. Omidvar, A. Amanati Shahri, A. L. C. Serrano, J. Gruber and G. Pamplona Rehder, *Sensors*, 2022, **22**, 8648.
28 W. Zheng, M. Zhao, W. Liu, S. Yu, L. Niu, G. Li, H. Li and W. Liu, *J. Electroanal. Chem.*, 2018, **813**, 75.
29 I. Fakih, O. Durnan, F. Mahvash, I. Napal, A. Centeno, A. Zurutuza, V. Yargeau and T. Szkopek, *Nat. Commun.*, 2020, **11**, 3226.
30 W. Fu, C. Nef, O. Knopfmacher, A. Tarasov, M. Weiss, M. Calame and C. Schönenberger, *Nano Lett.*, 2011, **11**, 3597.
31 W. Lee, S.-h. Jeong, Y.-W. Lim, H. Lee, J. Kang, H. Lee, I. Lee, H.-S. Han, S. Kobayashi, M. Tanaka and B.-S. Bae, *Sci. Adv.*, 2021, **7**, eabi6290.
32 J. Liu, J. Qian, M. Adil, Y. Bi, H. Wu, X. Hu, Z. Wang and W. Zhang, *Microsyst. Nanoeng.*, 2024, **10**, 57.
33 M. Xue, C. Mackin, W.-H. Weng, J. Zhu, Y. Luo, S.-X. L. Luo, A.-Y. Lu, M. Hempel, E. McVay, J. Kong and T. Palacios, *Nat. Commun.*, 2022, **13**, 5064.
34 H. G. Oh, D. C. Jeon, M. S. Gianti, H. S. Cho, D. A. Jo, M. N. Indriatmoko, B. K. Jang, J. M. Lim, S. Cho and K. S. Song, *Nanomaterials*, 2021, **11**, 787.
35 Y. Tahara and K. Toko, *IEEE Sens. J.*, 2013, **13**, 3001.
36 M. Podrazka, E. Báczyńska, M. Kundys, P. S. Jeleń and E. W. Nery, *Biosensors*, 2018, **8**, 3.
37 C. W. Lee, T. H. Eom, S. H. Cho and H. W. Jang, *Adv. Sens. Res.*, 2023, **2**, 9.
38 P. Traiwatcharanon, W. Siriwatcharapiboon and C. Wongchoosuk, *Chemosensors*, 2020, **8**, 58.
39 M. Naguib, O. Mashtalir, J. Carle, V. Presser, J. Lu, L. Hultman, Y. Gogotsi and M. W. Barsoum, *ACS Nano*, 2012, **6**, 1322.
40 S. Choudhury, D. Deepak, G. Bhattacharya, J. McLaughlign and S. S. Roy, *Macromol. Mater. Eng.*, 2023, **308**, 2300007.
41 P. K. Ang, W. Chen, A. T. S. Wee and P. L. Kian, *J. Am. Chem. Soc.*, 2008, **130**, 14392.
42 I. Meric, M. Y. Han, A. F. Young, B. Ozyilmaz, P. Kim and K. L. Shepard, *Nat. Nanotechnol.*, 2008, **3**, 654.
43 S. K. Cho and W. J. Cho, *Sensors*, 2021, **21**, 4213.
44 M. Wipf, R. L. Stoop, A. Tarasov, K. Bedner, W. Fu, I. A. Wright, C. J. Martin, E. C. Constable, M. Calame and C. Schönenberger, *ACS Nano*, 2013, **7**, 5978.
45 A. Cazalé, W. Sant, J. Launay, F. Ginot and P. Temple-Boyer, *Sens. Actuators, B*, 2013, **177**, 515.
46 K. Ito, H. Satake, Y. Mori, A. C. Tseng and T. Sakata, *Sci. Technol. Adv. Mater.*, 2019, **20**, 917.
47 H. R. Lim, Y. S. Kim, S. Kwon, M. Mahmood, Y. T. Kwon, Y. Lee, S. M. Lee and W. H. Yeo, *Sensors*, 2020, **20**, 3297.
48 N. Lei, P. Li, W. Xue and J. Xu, *Meas. Sci. Technol.*, 2011, **22**, 107002.
49 Z. Cheng, Q. Li, Z. Li, Q. Zhou and Y. Fang, *Nano Lett.*, 2010, **10**, 1864.
50 Y. Ohno, K. Maehashi, Y. Yamashiro and K. Matsumoto, *Nano Lett.*, 2009, **9**, 3318.
51 N. Dontschuk, A. Stacey, A. Tadich, K. J. Rietwyk, A. Schenk, M. T. Edmonds, O. Shimoni, C. I. Pakes, S. Prawer and J. Cervenka, *Nat. Commun.*, 2015, **6**, 6563.
52 S. S. Kwon, J. Yi, W. W. Lee, J. H. Shin, S. H. Kim, S. H. Cho, S. Nam and W. Il Park, *ACS Appl. Mater. Interfaces*, 2016, **8**, 834.
53 Y. Zhu, C. Wang, N. Petrone, J. Yu, C. Nuckolls, J. Hone and Q. Lin, *Appl. Phys. Lett.*, 2015, **106**, 123503.

54 B. Mailly-Giacchetti, A. Hsu, H. Wang, V. Vinciguerra, F. Pappalardo, L. Occhipinti, E. Guidetti, S. Coffa, J. Kong and T. Palacios, *J. Appl. Phys.*, 2013, **114**, 084505.
55 W. Liao, W. Wei, Y. Tong, W. K. Chim and C. Zhu, *ACS Appl. Mater. Interfaces*, 2018, **10**, 7248.
56 J. Luo, S. Jiang, H. Zhang, J. Jiang and X. Liu, *Anal. Chim. Acta*, 2012, **709**, 47.
57 C. Shan, H. Yang, D. Han, Q. Zhang, A. Ivaska and L. Niu, *Biosens. Bioelectron.*, 2010, **25**, 1070.
58 H. Wu, J. Wang, X. Kang, C. Wang, D. Wang, J. Liu, I. A. Aksay and Y. Lin, *Talanta*, 2009, **80**, 403.
59 Y. Huang, X. Dong, Y. Shi, C. M. Li, L. J. Li and P. Chen, *Nanoscale*, 2010, **2**, 1485.
60 Y. Wang, Y. Shao, D. W. Matson, J. Li and Y. Lin, *ACS Nano*, 2010, **4**, 1790.
61 G. H. Wu, X. H. Song, Y. F. Wu, X. M. Chen, F. Luo and X. Chen, *Talanta*, 2013, **105**, 379.
62 M. J. Kim, D. J. Han, G. E. Choi, R. Y. Park and D. W. Park, *J. Sens. Sci. Technol.*, 2024, **33**, 474.
63 Z. Zhao, Y. Song, Y. Xu, H. Hao, Y. Jin and Q. Wang, *Plasmonics*, 2025, **20**, 1073.
64 R. Devi, S. Gogoi, S. Barua, H. Sankar Dutta, M. Bordoloi and R. Khan, *Food Chem.*, 2019, **276**, 350.
65 J. H. Park, S. M. Joo, T. M. Kim, Y. Kim and H. H. Kim, *Electron. Mater. Lett.*, 2024, **20**, 818.
66 D. H. Kim, W. H. Park, H. G. Oh, D. C. Jeon, J. M. Lim and K. S. Song, *Sensors*, 2020, **20**, 4184.
67 V. Mazánek, O. Jankovský, J. Luxa, D. Sedmidubský, Z. Janoušek, F. Šembera, M. Mikulics and Z. Sofer, *Nanoscale*, 2015, **7**, 13646.
68 W. Fu, C. Nef, A. Tarasov, M. Wipf, R. Stoop, O. Knopfmacher, M. Weiss, M. Calame and C. Schönenberger, *Nanoscale*, 2013, **5**, 12104.
69 J. T. Robinson, J. S. Burgess, C. E. Junkermeier, S. C. Badescu, T. L. Reinecke, F. K. Perkins, M. K. Zalalutdniov, J. W. Baldwin, J. C. Culbertson, P. E. Sheehan and E. S. Snow, *Nano Lett.*, 2010, **10**, 3001.
70 N. Elgrishi, K. J. Rountree, B. D. McCarthy, E. S. Rountree, T. T. Eisenhart and J. L. Dempsey, *J. Chem. Educ.*, 2018, **95**, 197.
71 P. L. Runnels, J. D. Joseph, M. J. Logman and R. M. Wightman, *Anal. Chem.*, 1999, **71**, 2782.
72 B. Rajagopalan, S. H. Hur and J. S. Chung, *Nanoscale Res. Lett.*, 2015, **10**, 1.
73 S. Dutta, A. Dutta Chowdhury, S. Biswas, E. Y. Park, N. Agnihotri, A. De and S. De, *Biochem. Eng. J.*, 2018, **140**, 130.
74 N. Maity, A. Mandal and A. K. Nandi, *J. Mater. Chem. C*, 2017, **5**, 12121.
75 W. Li, Y. Zhang, C. Zhang, Q. Meng, Z. Xu, P. Su, Q. Li, C. Shen, Z. Fan, L. Qin and G. Zhang, *Nat. Commun.*, 2016, **7**, 11315.
76 T. Lee, H. L. Lee, M. H. Tsai, S.-L. Cheng, S.-W. Lee, J.-C. Hu and L.-T. Chen, *Biosens. Bioelectron.*, 2013, **43**, 56.
77 X. Zhang, Y. Zhang, W. Guo, K. Wan, T. Zhang, J. Arbiol, Y.-Q. Zhao, C.-L. Xu, M. Xu and J. Fransaer, *Mater. Adv.*, 2020, **1**, 908.
78 H. D. Duong, J. Kim and J. Il Rhee, *J. Sens. Sci. Technol.*, 2024, **33**, 70.
79 Y. Lu, Y. Xu, M. Lu, Y. Zhou, M. Li, Y. Feng and J. Wang, *IEEE Sens. J.*, 2024, **24**, 23901.
80 S. J. Park, S. M. Lee, M.-H. Oh, Y. S. Huh and H. W. Jang, *Sustainable Food Technol.*, 2024, **2**, 266.
81 S. M. Lee, Y. J. Kim, S. J. Park, W. S. Cheon, J. Kim, G. B. Nam, Y. Kim and H. W. Jang, *Adv. Funct. Mater.*, 2025, **35**, 2417019.
82 H. Liang, Y. Luo, Y. Xiao, R. Chen, L. Wang and Y. Song, *Ceram. Int.*, 2024, **50**, 977.
83 J. Y. Yue, X. L. Ding, L. Wang, R. Yang, J. S. Bi, Y. W. Song, P. Yang, Y. Ma and B. Tang, *Mater. Chem. Front.*, 2021, **5**, 3859.
84 X. Xuan, H. S. Yoon and J. Y. Park, *Biosens. Bioelectron.*, 2018, **109**, 75.
85 S. A. Lee, J. W. Yang, S. Choi and H. W. Jang, *Exploration*, 2021, **1**, 20210012.
86 M. A. Brown, Z. Abbas, A. Kleibert, R. G. Green, A. Goel, S. May and T. M. Squires, *Phys. Rev. X*, 2016, **6**, 1.
87 Y. W. Chen, C. R. Jhan, S. Neidle and M. H. Hou, *Angew. Chem., Int. Ed.*, 2014, **53**, 10682.
88 A. L. Lieblein, M. Krämer, A. Dreuw, B. Fürtig and H. Schwalbe, *Angew. Chem., Int. Ed.*, 2012, **51**, 4067.
89 Z. Wang, J. Zhao, Z. Li, J. Bao and Z. Dai, *Anal. Chem.*, 2017, **89**, 6815.
90 R. Li, M. Zhen, M. Guan, D. Chen, G. Zhang, J. Ge, P. Gong, C. Wang and C. Shu, *Biosens. Bioelectron.*, 2013, **47**, 502.
91 G. Ozcelikay, S. I. Kaya, E. Ozkan, A. Cetinkaya, E. Nemutlu, S. Kır and S. A. Ozkan, *TrAC, Trends Anal. Chem.*, 2022, **146**, 116487.
92 G. Li, X. Qi, J. Wu, L. Xu, X. Wan, Y. Liu, Y. Chen and Q. Li, *J. Hazard. Mater.*, 2022, **436**, 129107.
93 G. Kumar, V. P. Singh and S. K. Pandey, *Trans. Electr. Electron. Mater.*, 2024, **25**, 653.
94 H. H. Jung, J. Yea, H. Lee, H. N. Jung, J. Jekal, H. Lee, J. Ha, S. Oh, S. Song, J. Son, T. S. Yu, S. Jung, C. Lee, J. Kwak, J. P. Choi and K. I. Jang, *ACS Appl. Mater. Interfaces*, 2023, **15**, 46041.
95 C. M. Nguyen, W. D. Huang, S. Rao, H. Cao, U. Tata, M. Chiao and J. C. Chiao, *IEEE Sens. J.*, 2013, **13**, 3857.
96 X. Yang and J. C. Chiao, *IEEE Sens. J.*, 2018, **1**, 1.
97 R. Rahimi, M. Ochoa, T. Parupudi, X. Zhao, I. K. Yazdi, M. R. Dokmeci, A. Tamayol, A. Khademhosseini and B. Ziaie, *Sens. Actuators, B*, 2016, **229**, 609.
98 N. S. Kamarozaman, N. Zainal, M. A. Zulkefle, R. A. Rahman, A. B. Rosli, S. H. Herman and Z. Zulkifli, *Trans. Electr. Electron. Mater.*, 2024, **25**, 411.
99 N. Moser, C. Panteli, K. Fobelets and P. Georgiou, *Sens. Actuators, B*, 2019, **292**, 297.
100 S. Honda, M. Shiomi, T. Yamaguchi, Y. Fujita, T. Arie, S. Akita and K. Takei, *Adv. Electron. Mater.*, 2020, **6**, 1.
101 A. Repoulias, I. Logothetis, D. Matsouka and S. Vassiliadis, Electron, *Mater. Lett.*, 2024, **20**, 283.
102 T. Zhao, Q. Wang and A. Du, *Sensors*, 2021, **21**, 1.